Characterizing Ice Nucleating Particles over the Southern Ocean using Simultaneous Aircraft and Ship Observations

Kathryn A. Moore[1], Thomas C. J. Hill[1], Christina S. McCluskey[2], Cynthia H. Twohy[3,4], Bryan Rainwater[5*], Darin W. Toohey[5], Kevin J. Sanchez[6], Sonia M. Kreidenweis[1], and Paul J. DeMott[1]

[1]Department of Atmospheric Science, Colorado State University, Fort Collins, CO, USA
[2]Climate Global Dynamics Laboratory, NCAR, Boulder, Colorado
[3]NorthWest Research Associates, Redmond, WA, USA
[4]Scripps Institution of Oceanography, University of California, San Diego, CA, USA,
[5]Department of Atmospheric and Oceanic Sciences, University of Colorado, Boulder, CO, USA
[6]NASA Langley Research Center, Hampton VA, USA

Corresponding author: Kathryn Moore (kathryn.a.moore@colostate.edu)
[*]Now at: Handix Scientific Inc., Fort Collins, CO, USA

Key Points:

- First vertically resolved measurements of ice nucleating particles over the Southern Ocean, including in-cloud observations
- Correlation between normalized ice nucleating particle concentrations and wind speed suggests marine active site density is variable
- Higher ice nucleation efficiency observed above cloud, consistent with an increasing influence of mineral dust with height

Abstract

Supercooled liquid clouds are ubiquitous over the Southern Ocean (SO), even to temperatures below -20 °C, and comprise a large fraction of the marine boundary layer (MBL) clouds. Earth system models and reanalysis products have struggled to reproduce the observed cloud phase distribution and occurrence of cloud ice in the region. Recent simulations found the microphysical representation of ice nucleation and growth has a large impact on these properties, however, measurements of SO ice nucleating particles (INPs) to validate simulations are sparse. This study presents measurements of INPs from simultaneous aircraft and ship campaigns conducted over the SO in austral summer 2018, which include the first in situ observations in and above cloud in the region. Our results confirm recent observations that INP concentrations are uniformly lower than measurements made in the late 1960s. While INP concentrations below and above cloud are similar, higher ice nucleation efficiency above cloud supports model inferences that the dominant INP composition varies with height. Model parameterizations based solely on aerosol properties capture the mean relationship between INP concentration and temperature but not the observed variability, which is likely related to the only modest correlations observed between INPs and environmental or aerosol metrics. An updated parameterization for marine INPs is proposed, which reduces bias relative to existing methods by including wind speed as an additional variable. Direct and indirect inference of marine INP size suggests MBL INPs, at least those in the sub-2.5 μm range, are dominated by particles with diameters smaller than 500 nm.

Plain Language Summary

Although Antarctica is remote, the continent and the Southern Ocean that surrounds it play a fundamental role in shaping regional and global climate. The clouds in this region are unique, with less ice and more liquid water present at low temperatures than in other areas. This is likely related to very low concentrations of rare aerosol particles called ice nucleating particles, which cause liquid water droplets in clouds to freeze. Largely due to a lack of observations, Southern Ocean clouds are poorly represented in global models, and the interactions between aerosol particles and clouds are one of the largest remaining uncertainties. This study presents results of ice nucleating particle measurements from several recent field campaigns over the Southern Ocean, including the first observations within and above clouds in the region. Our results suggest different types of particles are present below and above clouds, which have varying ability to nucleate ice. They also highlight the need for additional measurements of ice nucleating particle composition and size, which are key variables needed to improve model simulations.

1 Introduction

The Southern Ocean (SO) surrounding Antarctica is frequently covered by vast tracts of low-level clouds, which have emerged as a key component in simulating regional and global climate, particularly the regional radiative budget (e.g. Bodas-Salcedo et al., 2013, 2016; Frey & Kay, 2017; Gettelman et al., 2020; Tan et al., 2016). Satellite retrievals suggest a greater occurrence of mixed-phase clouds containing supercooled liquid water (SLW) over the SO than at equivalent latitudes in the Northern Hemisphere (Chubb et al., 2013; Morrison et al., 2011), and recent in situ observations confirmed the ubiquity of supercooled liquid clouds and lack of ice to -20 °C (McFarquhar et al., 2021). In situ observations, although limited, also indicate more frequent drizzle and less ice over the SO compared to Arctic supercooled and mixed-phase clouds (Chubb

et al., 2013). Additionally, non-precipitating liquid clouds over the SO have higher cloud droplet number concentrations, smaller effective radii, and larger liquid water paths than subtropical stratocumulus (Mace et al., 2020). Despite observed differences between SO and Northern Hemisphere clouds, almost all model parameterizations have been developed with Northern Hemisphere data due to the lack of direct observations over the SO (Bromwich et al., 2012).

Until recently, earth system models, including those participating in CMIP5 (Coupled Model Intercomparison Project Phase 5), and reanalysis products overestimated the occurrence of ice and had insufficient liquid cloud cover over the SO, leading to a large shortwave radiation bias in the region (Bodas-Salcedo et al., 2013; Gettelman et al., 2020; Kay, Bourdages, et al., 2016; Kay, Wall, et al., 2016; Naud et al., 2014). This imbalance was hypothesized to be due to over-prediction of cloud glaciation and ice precipitation processes (Frey & Kay, 2017; Kay, Bourdages, et al., 2016; Mace et al., 2020; McFarquhar et al., 2021; Tan et al., 2016; Vergara-Temprado et al., 2018). Improvements in individual CMIP6 (Coupled Model Intercomparison Project Phase 6) models increased SLW and reduced radiation biases, improving agreement with observations (Bodas-Salcedo et al., 2019; Gettelman et al., 2020). Updated model representations of clouds are also responsible for higher equilibrium climate sensitivities (ECS) in many CMIP6 models compared to their CMIP5 counterparts due to corresponding changes in shortwave cloud forcing, likely driven by increases in SLW in CMIP6 models (Zelinka et al., 2020). The cloud phase feedback over the Southern Ocean is anticipated to strongly influence simulated future ECS (Bjordal et al., 2020), so understanding processes that affect cloud phase in this region is critical.

Cloud condensation nuclei (CCN) and ice nucleating particle (INP) budgets and sources for the SO are not fully constrained, although the dominant source for CCN is local (Humphries et al., 2021; Quinn et al., 2017; Twohy et al., 2021). The typically small droplet numbers of low marine clouds make them sensitive to changes in aerosol concentration, size, and source. Low INP concentrations, coupled with scavenging and deposition in drizzle, can limit primary ice production and contribute to high supercooling in liquid and mixed phase clouds. This has been observed in several marine regions in the Northern Hemisphere (Rosenfeld et al., 2013), and may also be occurring in the Southern Ocean. Vergara-Temprado et al. (2018) provided support for this hypothesis using the United Kingdom Met Office Global Unified Model, based on modeled INP concentrations. Secondary ice production has been observed in SO clouds >-25 °C, with sometimes large discrepancies between measured ice crystal and INP number concentrations. However, a large proportion of clouds do not contain measurable ice concentrations (Järvinen et al., 2022). Due to the potentially large role INPs may play in SO cloud phase, with downstream effects including cloud lifetime, precipitation, radiation budgets, and even ECS, understanding variability in the number and sources of INPs is crucial in this region.

Historically, INPs have been thought of as large, insoluble particles with surface structures that have specific sites that promote the freezing of ice (Pruppacher & Klett, 2010). These sites, known as active sites, typically scale with particle surface area and so are more numerous in larger particles (see Kanji et al., 2017). This approach has been used to derive model parameterizations for ice nucleation as a function of activation temperature by normalizing INP concentrations with a more commonly measured value, such as particle surface area or number concentration (e.g. DeMott et al., 2010, 2015; Hoose & Möhler, 2012; Kanji et al., 2017; McCluskey, Ovadnevaite, et al., 2018; Niemand et al., 2012; Ullrich et al., 2017). This approach requires the aerosol type or mixture to be known, since INP efficiency varies widely among particles of differing composition (e.g. Kanji et al., 2017). Strong relationships between INP

concentrations and particles >0.5 μm have been observed for mineral dust (DeMott et al., 2015), which is supported by the dominant supermicron mode of mineral and soil dust size distributions (Maring et al., 2003). Increasing awareness and study of additional categories of INPs, such as biological ice nucleators, which can be soluble and/or as small as ~10 nm, has challenged these assumptions about INP prerequisites (e.g. Kanji et al., 2017; Pummer et al., 2015; Wilson et al., 2015).

On a global scale, mineral and soil dusts are the dominant heterogeneous INP types in the immersion freezing mode due to their efficient ice nucleating ability (Hoose & Möhler, 2012; Testa et al., 2021) and high emission rates (Ginoux et al., 2012). Marine INPs have been identified as a distinct category (see DeMott et al., 2016), and shown to include marine diatoms and their exudates (Rosinski et al., 1987; Wilson et al., 2015), as well as marine macromolecules (McCluskey, Hill, Sultana, et al., 2018). Very recent laboratory studies indicate supermicron aerosol may be an important marine INP (Mitts et al., 2021), however, no assessment of the atmospheric transport of such particles was conducted and ambient observations have yet to confirm this. Marine INP number concentrations are generally 2-3 orders of magnitude or more lower than continental measurements (DeMott et al., 2016), as are marine INP active site densities (McCluskey, Ovadnevaite, et al., 2018).

Measurements of SO INPs are sparse, with initial measurements conducted by Bigg (1973, 1990), and the remainder comprised of data from several cruises, one aircraft campaign, and one study at the Australian Antarctic Division's (AAD) Macquarie Island station, all in the last decade (Kremser et al., 2021; McCluskey, Hill, Humphries, et al., 2018; McFarquhar et al., 2021; Miyakawa et al., 2023; Schmale et al., 2019; Tatzelt et al., 2022; Welti et al., 2020). Many of the measurements were also limited to the surface and to INPs active at temperatures of -15 or -20 °C due to either instrumental constraints or a particular focus on warmer mixed phase clouds (Welti et al., 2020). All of the measurements from the 1980s onwards are at the lower bound of those reported from other ocean regions (DeMott et al., 2016; Welti et al., 2020). There is now a consensus, supported by the observed low INP numbers, its remote location, and modeling studies (Burrows et al., 2013; McCluskey et al., 2019; Vergara-Temprado et al., 2017), that the SO INP population in the marine boundary layer is dominated by sea spray aerosol (SSA) and distinct from that found in the Northern Hemisphere. This is unlike the northern high latitudes, where mineral dust has been shown to dominate over locally sourced marine INPs in regions such as the Canadian Arctic (Irish et al., 2019).

2 Methods

2.1 Southern Ocean Measurement Campaigns

Measurements presented in this study were collected during the Southern Ocean Cloud Radiation Aerosol Transport Experimental Study (SOCRATES, hereafter SOC) aircraft campaign and the second Clouds, Aerosols, Precipitation, Radiation and atmospherIc Composition Over the southeRN ocean (CAPRICORN-2, hereafter CAP-2) ship campaign. Both campaigns were conducted simultaneously during Austral summer (January-March) 2018, based out of Hobart, Tasmania and are fully described in McFarquhar et al. (2021). SOC measurements utilized the NSF/NCAR G-V aircraft (UCAR/NCAR - Earth Observing Laboratory, 2005) and collected cloud microphysical and aerosol observations within the marine boundary layer (MBL) and up to the free troposphere as far south as 62°S. CAP-2 collected complementary MBL measurements aboard the RV *Investigator* (voyage IN2018_V01), an Australian Government research platform operated by the Commonwealth Science and Industrial Research Organisation

(CSIRO). A map indicating the locations of the 15 SOC research flights and the CAP-2 track are given in Fig. S1. The SOCRATES campaign is noteworthy for collecting the first in situ observations of INPs in and above cloud in this region.

2.2 Aerosol Measurements

The collection and analysis of particle size distribution measurements during CAP-2 and SOC were fully described in Moore et al. (2022) and will only be briefly covered here. Integrated particle number, surface area, and volume concentrations are used as normalization metrics and inputs to parameterizations for estimating INP concentrations, as discussed in Sec. 3.2. Measurements of single particle composition during SOC using offline elemental analysis (Twohy et al., 2021) are similarly used as parameterization inputs (Sec. 3.4).

2.2.1 CAPRICORN-2 Aerosol Size Distributions

Particle size distributions were generated by merging observations from a TSI Scanning Mobility Particle Sizer (TSI, SMPS 3080; 15-660 nm) and a TSI Aerodynamic Particle Sizer (TSI, APS 3320; 500 nm – 20 μm) averaged over 30-min intervals. Silica gel diffusion driers were used to dry particle streams to below the efflorescence relative humidity (ERH) of sea salt (45-48%; Tang et al., 1997) and the resulting particle data are described as "dry" throughout this manuscript. SMPS and APS sizes were converted from their native mobility and aerodynamic diameters, respectively, to volume equivalent diameters prior to merging (Moore et al., 2022). Ship exhaust and waste incineration represent the largest sources of particle contamination for aerosol measurements on the RV *Investigator* and were excluded from the data set using a time series of predicted exhaust influence on measurements following Humphries et al. (2019). Theoretical particle transmission efficiency calculations (Moore et al., 2022) were applied to merged size distributions to correct for primarily supermicron particle losses inside the RV *Investigator* aerosol sampling inlet. Distributions were cut off at 5 μm dry diameter, as above this size the theoretical transmission efficiency drops below 40% and the correction becomes highly uncertain. Three-four lognormal modes were fit to the resulting merged distributions following Quinn et al. (2017) and Modini et al. (2015), and primary marine aerosol (PMA) estimated as the sum of the third and fourth (if applicable) coarse modes (Moore et al., 2022). Integrated particle number, surface area, and volume concentrations were then calculated for each total distribution and the PMA modes, assuming spherical particles. Comparison of total integrated quantities with those for particles <5 μm from the G-V measurements (see Sec. 2.2.2), which were obtained from wing-mounted instruments with minimal or no inlet losses, were used to derive additional corrections for losses not accounted for in the CAP-2 inlet modeling. These corrections were applied to all CAP-2 integrated aerosol measurements presented here. Due to a lack of available nephelometer data for CAP-2, theoretical scattering distributions at 450 nm, 525 nm, and 635 nm were estimated for each size distribution using Mie theory, using a refractive index of n=1.5 (Tang et al., 1997) and assuming spherical particles (Moore et al., 2022). Ångström exponents (å) were then calculated for each wavelength pair from the integrated scattering coefficients. Blue/red å<=0.8 was found to work well as a tracer for aerosol size distributions dominated by primary marine aerosol during CAP-2 (Moore et al., 2022), which will be discussed further in Sec. 3.1.

2.2.2 SOCRATES Aerosol Size Distributions

Average aerosol distributions were generated by merging observations from a wing-mounted ultra-high sensitivity aerosol spectrometer (Droplet Measurement Technologies, UHSAS; 0.06 –

1.0 μm) and a wing-mounted cloud droplet probe (Droplet Measurement Technologies, CDP; 1-50 μm; Lance et al., 2010). For some distributions, primarily in the MBL, measurements of supermicron particles from the Giant Nucleus Impactor (GNI; Jensen et al., 2020) were also available. UHSAS distributions were considered to represent dry particles due to the use of deicing heaters that lowered the RH in the optical cavity to <40% (Moore et al., 2022; Sanchez, Roberts, et al., 2021). The GNI technique involves collection of impacted particles onto glass slides, followed by microscopic imaging to calculate the spherical-equivalent dry sizes of collected particles (Jensen et al., 2020). CDP bin sizes were first adjusted following Lance et al. (2010) and then corrected for water uptake using hygroscopic growth factors calculated for sea salt proxies using E-AIM (Clegg et al., 1998, 2021). Following the same method as the CAP-2 observations, after merging the UHSAS, CDP, and GNI data (if available), each distribution was fit with lognormal modes and PMA estimated, although the Aitken mode was ignored in the SOC measurements because the UHSAS doesn't extend to small enough sizes to constrain it.

The distributions presented in Moore et al. (2022) represented averages of ~8-10 min level legs in the lower MBL (150-300 m MSL). Additional level legs above cloud and in the upper troposphere (>5000 m) were identified in this study during INP observation periods (Sec. 3.4). For INP observations less than 10 min in duration, level legs up to 10 min were identified where "level legs" were defined as periods with <5% deviation from the midpoint altitude, based on the INP measurement period. For INP observations longer than 10 min in duration, aerosol measurements were averaged over the INP measurement period regardless of altitude variations so that all observed variability was captured in both measurements. To avoid cloud contamination of the aerosol distributions, any points with cloud condensed water >0.01 g m^{-3} were removed prior to averaging. Estimates of cloud condensed water were made with several instruments during SOCRATES; here we define "in-cloud" periods when either the wing-mounted CDP or tunable diode laser hygrometer, which sampled behind a counterflow virtual impactor inside the G-V cabin (CVI; Noone et al., 1988; Twohy et al., 2010) reported cloud condensed water >0.01 g m^{-3}.

Since PMA estimates based on lognormal mode fitting alone are unlikely to be meaningful outside of the MBL, merged distributions for the above cloud and upper troposphere periods were instead generated by first applying a lowpass (smoothing) filter to the average UHSAS, CDP, and GNI (if available) distributions to reduce noise. Then, a smoothing spline was fit to the smoothed distributions, interpolating onto the same logarithmically spaced bins as the lognormal fits to the MBL distributions described in Moore et al. (2022). The merging process was conducted using surface area distributions, since they are more sensitive in the size region between the UHSAS and CDP or GNI. Finally, integrated particle number, surface area, and volume were calculated for each distribution. The same procedure was applied to the MBL periods identified in Moore et al. (2022) and compared to the results of the lognormal fitting to verify both methods produce equivalent results. For both integrated surface area and number concentration of particles larger than 500 nm dry diameter (n500), points cluster around the 1:1 line, with maximum deviations of 57% for aerosol surface area and 67% for n500 (Fig. S2). Mie calculations were used to calculate theoretical scattering distributions and Ångström exponents (å) for each merged size distribution, following the same procedure as in Moore et al. (2022).

2.2.3 SOCRATES Aerosol Composition Analysis

Particles were collected via impaction onto carbon-coated electron microscope grids during SOCRATES in two dry diameter ranges: 0.1-0.5 μm and 0.5-5 μm, as fully described in Twohy

et al. (2021). Collections were made downstream of the CVI inlet in clear air below and above cloud, and of cloud droplet residuals in-cloud. Single-particle size, morphology, and elemental composition were determined with analytical Scanning Transmission Electron Microscopy (STEM) using Energy Dispersive X-ray Spectroscopy (EDS). Particles were then classified into 8 categories, including crustal/dust, sulfur, organic, metals, sea-spray with high sodium, and sea-spray with high sulfur content (Twohy et al., 2021). In this study, the sum of the crustal/dust and metal categories above and below cloud were used as parameterization inputs to estimate INP concentrations (Sec. 3.4).

2.3 Ice Nucleating Particle Observations

Measurements of INPs active in the immersion freezing mode were made in real time with Colorado State University (CSU) Continuous Flow Diffusion Chambers (CFDCs) at temperatures below -25°C, and via offline analyses of aerosol filter samples using the CSU Ice Spectrometer (IS) from -10 to -30°C. Ice crystals that activated within the CFDC were also collected and analyzed by STEM/EDS to assess the composition and size of INP residuals (Twohy et al., 2021).

2.3.1 Continuous Flow Diffusion Chamber Measurements

The Continuous Flow Diffusion Chamber (CFDC) is an online instrument used to measure primary INP number concentrations in an aerosol stream (DeMott et al., 2015; Rogers, 1988; Rogers et al., 2001). Two concentric, cylindrical walls are coated with ice and thermally controlled to establish a temperature and humidity gradient between the walls in the upper "growth" region of the chamber, allowing aerosol particles to activate into ice crystals and grow. The HIAPER (CFDC-1H) version of the CFDC used in SOC (Barry et al., 2021) and a duplicate version used during CAP-2 (McCluskey, Hill, Humphries, et al., 2018) both have total residence times of ~7 s based on their sample volumetric flow rate of 1.5 lpm. Ice crystals are detected optically with an OPC at the base of the chamber and distinguished by size from aerosol or activated cloud droplets. For both SOC and CAP-2, water supersaturated conditions, typically 104-108% RH, were maintained in the growth region, which forces activation of aerosols into cloud droplets prior to ice nucleation, giving results similar to offline immersion freezing techniques (DeMott et al., 2016). Prior to entering the chamber, the aerosol stream is dried to below the frost point, and supermicron aerosols that might interfere with optical detection of ice crystals are removed by passing the aerosol stream through two identical single-jet impactors in series. For SOC, impactors with a 2.4 μm cut size were used; during CAP-2 1.5 μm impactors were used to limit interferences from highly hygroscopic, supermicron sea spray aerosols. Low INP concentrations during both campaigns limited operating temperatures to -25°C and below, with the majority of measurements collected ~ -30°C. Measurement periods of approximately 10 minutes were alternated with 5-min periods measuring HEPA-filtered air to provide instrument background counts, which vary by operating temperature and environmental conditions. INP concentrations presented here have been background-corrected using adjacent filtered-air periods, as described in Moore (2020) and Barry et al. (2021). Calculation of confidence intervals and assessment of statistical difference between sample and background periods follow Krishnamoorthy and Lee (2012) and are also detailed in Moore (2020) and Barry et al. (2021). Concentrations are reported at standard conditions (STP; 0 °C and 100 kPa).

During CAP-2, the CFDC sampled from the same RV *Investigator* aerosol sampling inlet as the SMPS, APS, and other aerosol instrumentation (Moore et al., 2022). In addition to direct

ambient measurements, an aerosol concentrator (MSP Corporation Model 4240) was employed upstream of the CFDC to pre-concentrate ambient aerosol and enhance INP number concentrations prior to measurement, as in previous ground-based (Tobo et al., 2013) and ship-board (McCluskey, Hill, Humphries, et al., 2018) studies. The aerosol concentrator inlet was constructed from 1" stainless steel tubing and followed the same path as the main aerosol inlet down the RV *Investigator* foremast and into the aerosol lab at the bow of the ship. INP concentration factors for measurements made with the aerosol concentrator were calculated through comparison to ambient INP measurements made at the same temperature (±2 °C) and within 30 minutes. These concentration factors were used to scale measurements made with the aerosol concentrator to their equivalent ambient concentration. Theoretical particle transmission efficiency calculations for the CFDC ambient and concentrator inlets (Fig. S3; Brockmann, 2011; von der Weiden et al., 2009) indicate >90% for the ambient and >85% transmission efficiency for the concentrator inlet at sizes up to 1.5 μm, and so no particle loss corrections were applied to measured INP concentrations. Unlike the aerosol size distribution measurements (Sec. 2.2.1), the CFDC data were not filtered to exclude ship exhaust, as previous measurements have indicated very low IN efficiency of particles emitted from diesel engines (Schill et al., 2016), and inspection of INP concentrations showed no significant differences between adjacent measurements when one was influenced by ship exhaust and the other was not. This is consistent with previous ship-board measurements for temperatures above -26°C (Irish et al., 2019; McCluskey, Hill, Humphries, et al., 2018; Welti et al., 2020).

On the G-V, the CFDC sampled from both the HIAPER modular inlet (HIMIL inlet; Stith et al., 2009) in clear air regions above and below clouds, and from a counterflow virtual impactor (CVI) inlet within clouds (Noone et al., 1988; Twohy et al., 2010) to detect INPs within cloud residuals. Particle transmission efficiencies for the HIMIL inlet have been previously characterized as >94% for submicron particles (Stith et al., 2009), and no corrections were applied to the CFDC data, which has an upper limit of 2.4 μm aerodynamic diameter. CVI transmission efficiencies were modeled by Twohy et al. (2010) using computational fluid dynamics software, and used to correct the in-cloud CVI data presented here for particle enhancements in the inlet. Some measurements in cloud-adjacent regions were also made using the CVI inlet in clear air, with the counterflow turned off ("total mode"). CVI enhancements in total mode are highly size dependent, and expected to range from ~1.1-3.5 for the particle sizes sampled by the CFDC (Twohy et al., 2016). Since INP sizes during each measurement are unknown, but likely variable (Twohy et al., 2021), no correction has been applied to the total mode CVI measurements from SOCRATES.

2.3.2 Ice Spectrometer Measurements

Aerosols were collected onto pre-cleaned 0.2 μm, 47mm track-etched polycarbonate membrane filters (Whatman Nucleopore filters, GE Healthcare Life Sciences) in either pre-sterilized aluminum inline filter housings (Pall) on the G-V, or disposable, sterile, open-faced filter units (Nalgene sterile analytical filter units, Thermo Fisher Scientific) on the RV *Investigator*. During CAP-2, filters were mounted on deck beneath a rain hat for alternating 24 and 48 hr periods at approximately 23 m above sea level. In order to limit ship exhaust contamination, the filter pump was powered with a sector sampler, which provided power to the pump only when the wind speed relative to the ship was between 10 and 80 knots, the ship-relative wind direction was from the forward 90° (relative wind directions greater than 45° and less than 315° were excluded), and the total particle concentrations measured by a CPC were

stable and less than 2000 cm^{-3}. On the G-V, filters sampled from the same HIMIL as the CFDC (Sec. 2.3.1) above or below cloud. Due to the low INP concentrations, each SOC filter was collected for multiple, approximately level legs at similar altitudes, but different locations throughout a flight. Separate filters were collected in the MBL and above cloud to assess changes in INPs with altitude. Filters where >5% of the collection period was in-cloud based on cloud condensed water measurements (Sec. 2.2.2) have been excluded from results presented here. Filters were stored frozen (-80 °C) following collection and during transport (via a liquid nitrogen dry shipper) back to CSU, and at -20 °C thereafter. Blank filters were collected throughout the voyage and during the research flights and processed identically to the samples.

The CSU Ice Spectrometer (IS) was used to measure immersion freezing INP temperature spectra from liquid suspensions of particles collected onto filters during CAP-2 and SOC. The current version of the IS was described in Hiranuma et al. (2015) and DeMott et al. (2018). Aliquots of sample suspensions, typically 32 or 48 droplets of 50 μL, were dispensed into sterile 96-well PCR trays (Optimum Ultra, Life Science Products) and then placed into temperature-controlled aluminum blocks and cooled at approximately 0.33 °C min^{-1}. Freezing was detected optically using a CCD camera, with the number and position of frozen droplets (wells) recorded at 1 Hz. The minimum analysis temperature for each sample or blank was determined by comparison with a 0.1 μm-filtered DI water negative control and was typically between -27 and -30 °C. Calculations of INP concentrations in the liquid suspension were made following Vali (1971), which were then converted to concentrations in ambient air, expressed at standard conditions (STP; 0 °C and 100 kPa). Uncertainties are reported as binomial sampling confidence intervals (95%) as in Agresti and Coull (1998). The limit of detection (LOD) was taken as the upper 95% confidence interval for 0 droplets frozen out of a sample, corresponding to 3-4 frozen wells for these filter collections. As a result, samples were considered above the LOD once 4-5 wells had frozen, leading to an upper temperature limit of about -17 °C. Measured concentrations were corrected using the average background number of INPs from 6 (SOC) or 5 (CAP-2) blank filters and are not reported if blank-corrected values fell below zero.

An earlier version of the SOC IS filter dataset was presented in Järvinen et al. (2022) as a comparison to in-cloud measurements of ice crystal number concentrations, and the concentrations were used in McCluskey et al. (2023) and Zhao et al. (2023) to evaluate CAM6 INP predictions (Sec. 2.4). Preliminary CAP-2 filter results were shown in McFarquhar et al. (2021), along with previous measurements made in the Southern Ocean. The blank-correction procedure reported here represents an improved statistical methodology from what has been previously reported (e.g. Barry et al., 2021; DeMott, Möhler, et al., 2018), providing more accurate 95% confidence intervals on blank-corrected data and improved LOD estimations. The midpoint concentrations are identical to previous methodologies and are directly comparable.

2.3.3 INP Size and Composition Analysis

Following the OPC at the outlet of the CFDC chamber is a single-jet impactor with a 50% cut-size of 4 μm aerodynamic diameter, which was used to collect ice crystals that nucleated inside the CFDC chamber during both SOCRATES and CAPRICORN-2 (Barry et al., 2021; McCluskey et al., 2014). Similarly to the total particle collections during SOC (Sec. 2.2.3), the CFDC STEM impactor was fitted with Cu grids (coated with formvar and C), and the collected ice crystal residuals were analyzed with STEM/EDS to determine residual size, morphology, and composition (Twohy et al., 2021). In this study, only the size measurements of INPs will be discussed. Six samples from CAP-2 and four samples from SOC were collected, with collection

temperatures that ranged from -27 to -32 °C and n=87 total particles analyzed; the collection locations are shown in Twohy et al. (2021) Fig. 1. Since all the CAP-2 and the majority of the SOC INPs were collected in the MBL, the overall sample is expected to be dominated by particles from the MBL.

Indirect inference of INP sizes was also possible based on the INP concentration factors calculated from CAP-2 ambient CFDC measurements versus those made using the aerosol concentrator (Sec. 2.3.1). The aerosol concentrator primarily acts on particles >0.5 μm diameter, with a concentration factor that is highly size dependent up to ~1 μm aerodynamic diameter (Tobo et al., 2013). For particles 0.5-1 μm aerodynamic diameter, the measured INP concentration factor thus provides indirect evidence of INP size. Due to the very low INP concentrations present over the Southern Ocean MBL (Fig. 1), measurements of INP concentration factor were limited to <=-25 °C, and predominantly ~-30 °C. Concentration factors of the aerosol concentrator as a function of particle diameter were derived from sequential measurements of ambient aerosol particles with and without the aerosol concentrator upstream of an Aerodynamic Particle Sizer (TSI, APS 3321) for particles between 500 nm and 20 μm aerodynamic diameter. They are shown in Fig. S4, where the particle sizes have been converted from aerodynamic to physical dry diameter, using the APS diameter correction factor derived for CAP-2 particle measurements (Moore et al., 2022).

2.4 SOCRATES CAM6 Model Simulations

A simulation of aerosols during SOCRATES was conducted with the atmospheric component of CESM2 (Community Earth System Model version 2), CAM6 (Community Atmosphere Model version 6), as described and presented in McCluskey et al. (2023). The CAM6 simulation used the standard 32 vertical levels (surface to 3 hPa), a 30-min time step with 10-min microphysical sub-step, and horizontal resolution of 0.9° latitude by 1.25° longitude. It was performed using a "nudged", or specified dynamics, configuration, with winds and temperatures from the MERRA2 reanalysis product with a 24-hr relaxation timescale (Gettelman et al., 2020). For comparison to the in situ observations, CAM6 output were at 1-min resolution and co-located with the measurements using the G-V position and altitude to determine the nearest model gridbox. For co-locations with the IS measurements, model data were averaged along the G-V track during the filter collection period.

CESM2 uses the 2-moment modal aerosol model MAM4 (Liu et al., 2016), which includes six aerosol species: sea salt, mineral dust, black carbon (BC), primary organic matter (POM), sulfate, and secondary organic aerosol (SOA). Aerosols are emitted into 4 modes with contributions that vary by aerosol type, with a fixed modal width and a modal diameter that evolves during the simulations. Inorganic sea spray fluxes are estimated based on whitecap area as a function of wind speed (Monahan & Muircheartaigh, 1980) and sea surface temperature in two size ranges: 0.02 to 2.8 μm (Mårtensson et al., 2003) and 2.8-10 μm (Monahan et al., 1986). Mineral dust fluxes are based on wind speed and soil aridity (Zender et al., 2003), and both mineral dust and sea salt emissions are interactive with model meteorology. The remaining aerosol species (BC, POM, sulfate, and SOA) are emitted based on CMIP6 emission inventories (Gettelman et al., 2019). In this analysis, only out of cloud (ambient/interstitial) aerosol was used, and similarly to the observations (Sec. 2.2), aerosol surface area concentrations were calculated from the simulated number size distributions assuming spherical particles.

McCluskey et al. (2019, 2023) concluded the best approach for predicting INP concentrations over the Southern Ocean using CAM and existing parameterizations was to sum the sea spray

INP contribution using the marine organic aerosol parameterization (M18) from McCluskey et al. (2018) and the mineral dust INP contribution following the DeMott et al. (2015) parameterization (D15). The simulated CAM6 INP concentrations presented in this study use this approach. Simulated sea salt aerosol surface area concentrations and the number concentration of mineral dust particles larger than 500 nm were used as parameterization inputs for M18 and D15, respectively.

3 Results and Discussion

3.1 CAPRICORN-2 and SOCRATES Marine Boundary Layer INP Observations

The most comprehensive historical measurements of Southern Ocean INPs are those of Bigg (1973, 1990). Since then, measurements of INPs, primarily immersion freezing assays of aerosol filters, have been collected during several campaigns in different regions of the Southern Ocean, and are collated in Welti et al. (2020) and McFarquhar et al. (2021). As previously noted for the CAPRICORN-1 (2016; McCluskey, Hill, Humphries, et al., 2018) and Antarctic Circumnavigation Expedition (ACE, 2016-2017; Schmale et al., 2019; Tatzelt et al., 2022; Welti et al., 2020) campaigns, modern measurements are one to several orders of magnitude lower than the original observations presented in Bigg (1973). During CAP-2, average IS measurements of filters at -20 °C are approximately 2 orders of magnitude lower than those collected during 1969-1972 across all latitudes sampled. Measurements at temperatures above -15 °C from CAP-2 were below the detection limit, which prevents additional direct comparisons. Slightly elevated INP concentrations were observed at -25 °C during CAP-2 at the northern and southern ends of the voyage (not shown), though all latitudinally-averaged values agree within their estimated uncertainties. Future measurements should evaluate this latitudinal variability during seasons other than austral summer.

INP measurements collected in the marine boundary layer from both IS filters and CFDC observations during SOCRATES and CAPRICORN-2 are compiled in Fig. 1. As discussed in Sec. 2.3.2, the INP filter measurements included in this study represent updated versions of the datasets, with improved confidence interval and LOD estimates. All panels in Fig. 1 show INP observations as a function of temperature; Fig. 1a has measured INP concentrations and the remaining panels display INP concentrations normalized by measured aerosol concentration metrics for comparison to model parameterizations, which will be discussed further in Sec. 3.2. Normalization of INP concentration with particle number gives activated fraction, N_n (Fig. 1b), normalization with particle surface area gives the surface active site density, N_s (Fig. 1c), and normalization with particle volume gives the volume active site density, N_v (Fig. 1d). The activated fraction presented in this study uses the number concentration of aerosols larger than 500 nm (n500), which has been used in several previous INP model parameterizations (e.g. DeMott et al., 2015; Tobo et al., 2013). While the surface active site density is typically abbreviated as n_s, N_s will be used throughout this manuscript to distinguish it from n500. Best-fit exponential functions (black lines in Fig. 1b-d) are given by Equation 1:

$$N_x(T) = \exp(a \cdot T + b) \#(1)$$

where N_x is the activated fraction (N_{n500}), surface active site density (N_s), or volume active site density (N_v), T is temperature (°C), and a and b are fit parameters. Fit parameters and R^2 values

for functions shown in Fig. 1 are listed in Table S1. The median-lognormal fitting process suggested by Li et al. (2022) was attempted, but the relatively small number of available measurements at warm temperatures prevented robust estimates of the lognormal fit parameters. Instead, regression parameters were calculated with all the available data, using the least absolute residuals method to reduce the impact of extreme values far from the median (e.g. Bassett & Koenker, 1978).

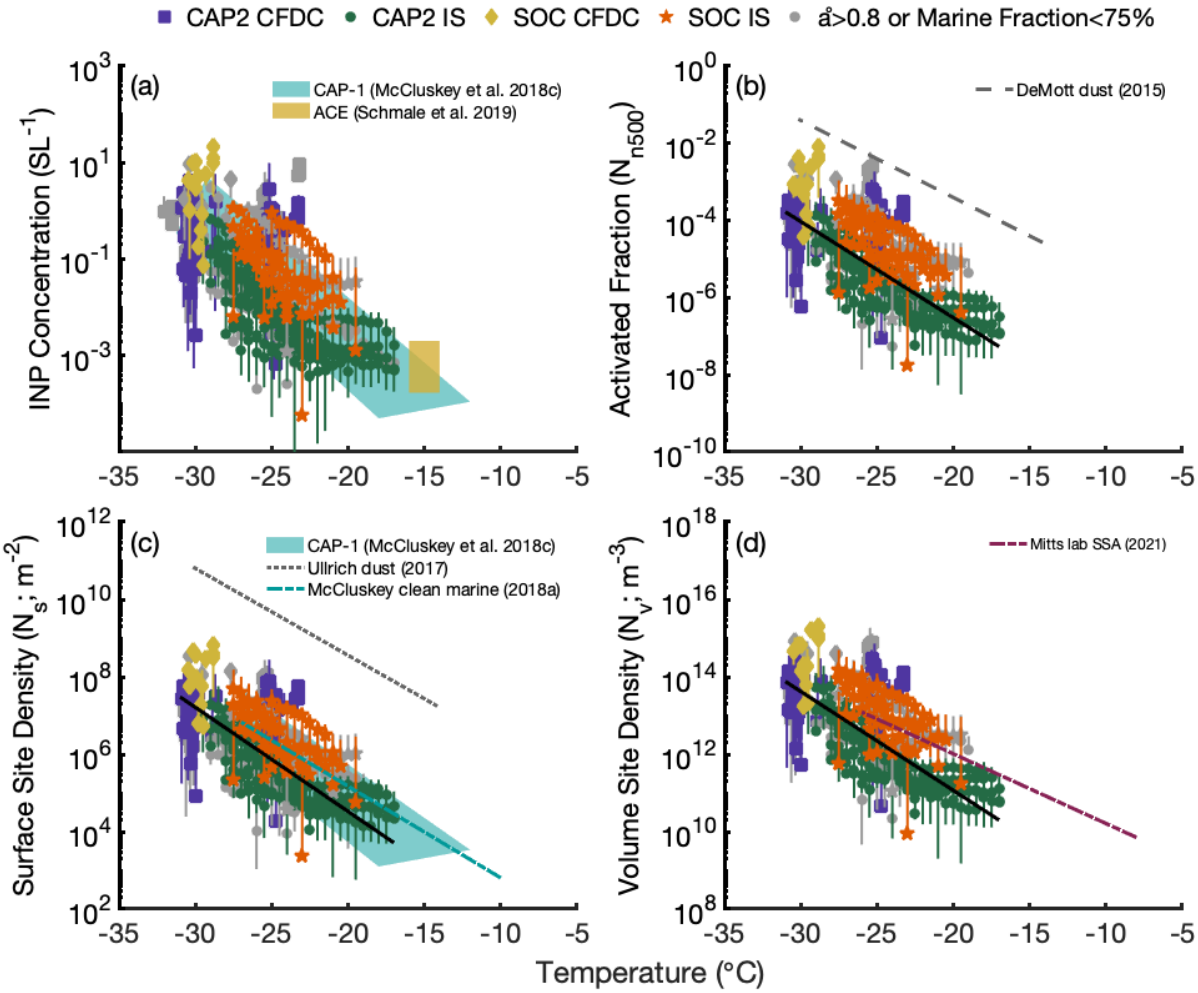

Figure 1. INP (a) number concentration, (b) normalized by n500 (N_{n500}), (c) normalized by aerosol surface area (N_s) and (d) normalized by aerosol volume (N_v) temperature spectra during SOC and CAP-2 in the MBL. CAP-2 CFDC (purple squares), CAP-2 filter (green circles), SOC CFDC (gold diamonds), and SOC filter (orange stars) are shown in (a), and in (b-d) when simultaneous aerosol observations were available for normalization. In (a) and (c), the blue shading indicates the range of values observed during CAPRICORN-1 (McCluskey, Hill, Humphries, et al., 2018). The gold shading in (a) shows observations made during the ACE campaign (Schmale et al., 2019). In (b), the grey dashed line shows the DeMott et al. (2015) parameterization for dust based on n500, using the mean n500 value observed during CAP-2. In (c), the grey dotted line indicates the Ullrich et al. (2017) parameterization for dust N_s, and the blue dot-dash line shows the N_s parameterization from McCluskey, Ovadnevaite, et al. (2018) for North Atlantic clean marine air. The dashed magenta line in (d) indicates the Mitts et al. (2021)

lab-based parameterization for marine N_v. Non-grey symbols have an å<=0.8 and 5-day back trajectory ocean fraction >75% to identify samples dominated by marine aerosol; grey symbols do not meet at least one of these criteria. Solid black lines in (b-d) indicate the best-fit exponential functions (Eq. 1, Table S1) to the non-grey symbols.

Good agreement is seen with previously published INP measurements from the Southern Ocean during the CAPRICORN-1 campaign (McCluskey, Hill, Humphries, et al., 2018; blue shading in Fig. 1a,c). Due to the more stringent blank-correction procedure applied to this IS dataset than previous ones (Sec. 2.3.2), there is no direct overlap with the warm-temperature results from ACE (Schmale et al., 2019; gold shading in Fig. 1a), although they are at the high end of those reported for CAPRICORN-1. Additional results from ACE presented in Welti et al. (2020) and Tatzelt et al. (2022) have not been included, as they were not corrected for field blanks, which are a significant fraction of the measured concentrations, particularly at colder temperatures (Tatzelt et al., 2022 Fig. S5 and S8). The lack of blank correction may also explain the higher INP concentrations reported from ACE measurements relative to those from CAPRICORN-1, CAP-2, and SOC, although differences in sampling time and location likely also play a role. Parameterizations for dust INPs based on global INP data and number concentrations of aerosols larger than 500 nm (DeMott et al., 2015) or aerosol surface area concentrations (Ullrich et al., 2017) overpredicted the observations from SOC and CAP-2, corroborating the growing consensus that the majority of boundary layer-INPs in this region are local, and of marine origin (Burrows et al., 2013; McCluskey et al., 2019, 2023; McCluskey, Hill, Humphries, et al., 2018; Vergara-Temprado et al., 2017; Welti et al., 2020). The N_s-based marine INP parameterization proposed by McCluskey, Ovadnevaite, et al. (2018) using data collected at Mace Head Research Station in Western Ireland is consistent with the exponential best-fit line derived using this dataset between -25 and -27 °C, but has an increasing high bias at warmer temperatures. The more conservative blank-correction procedures used for this study relative to past campaigns (Sec. 2.3.2) may have contributed to the lower slope obtained by McCluskey, Ovadnevaite, et al. (2018). Similarly, the Mitts et al. (2021) parameterization for N_v based on laboratory measurements has a lower slope than the fit derived from this dataset, and as a result was found to lie at or above the upper bound of CAP-2 and SOC measurements for temperatures warmer than -20 °C, and above the best fit line at all temperatures.

The role of air-mass history and particle source on INP observations was explored using Ångström exponent (å; Moore et al., 2022) and HYSPLIT (Rolph et al., 2017; Stein et al., 2015) back trajectories. å<=0.8 (Sec. 2.2.1) was previously found to work well as a tracer for aerosol size distributions dominated by primary marine aerosol during CAP-2, and was further supported by the degree of marine influence calculated from HYSPLIT back trajectories (Moore et al., 2022). The degree of marine influence was defined as the fraction of a 5-day back-trajectory that passed over the ocean (Sanchez, Zhang, et al., 2021). Non-grey points in Fig. 1 have both å<=0.8 and a HYSPLIT marine influence >75%; grey points did not meet at least one criterion to be considered marine-dominated. While these metrics worked well to classify SOC and CAP-2 aerosol measurements, there were no discernable differences in INP concentrations or normalized values for marine-dominated periods versus the remaining measurements. Similarly, using primary marine aerosol number, surface area, or volume (Fig. S5) to normalize INP concentrations produced the same results as using total quantities.

3.2 Parameterizing marine INP concentrations

For marine INPs, two parameterizations based on field measurements have been published; one uses aerosol surface area (M18; McCluskey, Ovadnevaite, et al., 2018), and the other SSA organic carbon mass (W15; Wilson et al., 2015) to predict INP concentrations, in addition to activation temperature. The TOC-based parameterization of Wilson et al. (2015) used INP measurements and organic carbon mass concentrations of sea surface microlayer (SML) samples from the Arctic and North Atlantic Oceans to estimate INPs in the organic component of sea spray aerosol. W15 was evaluated in McCluskey, Ovadnevaite, et al. (2018) for North Atlantic marine atmospheric INPs and found to overpredict INP concentrations at -15 and -20 °C by a factor of 4 to 100. Using the same observations, M18 developed an alternative parameterization based on measurements of ambient INPs in SSA at Mace Head, Ireland, which specifically aims to describe organic-coated sea salt particles and not INPs active at warm temperatures, which may be associated with microbes. Both W15 and M18 were evaluated using E3SMv1 (Energy Exascale Earth System Model version 1) simulations of INPs during the March 2016-March 2018 Macquarie Island Cloud Radiation Experiment (MICRE) campaign (Raman et al., 2023). Unlike for the CAPRICORN-1 and SOCRATES campaigns (McCluskey, 2022; McCluskey et al., 2019), W15 produced the best agreement with the MICRE atmospheric INP observations (DeMott, Hill, Marchand, et al., 2018; McFarquhar et al., 2021). However, MICRE observations were also found to be higher than those from open ocean SO measurements, including during ACE (Tatzelt et al., 2022) and the Measurements of Aerosols, Radiation, and Clouds over the Southern Ocean (MARCUS) campaign (DeMott, Hill, & McFarquhar, 2018; McFarquhar et al., 2021). This discrepancy is likely due to local processes enhancing INP concentrations at Macquarie Island (Raman et al., 2023). Since SOC and CAP-2 measurements are in good agreement with those from CAPRICORN-1, and W15 predicts higher INP concentrations than M18, we adopt the approach of McCluskey et al. (2019, 2023) and use M18 instead of W15 here. Very recent laboratory experiments suggest that for marine INPs, the active site density may be proportional to particle volume rather than surface area (Mitts et al., 2021), however, field confirmation of this is lacking.

The utility of different normalizations for predicting INP concentrations over the SO are demonstrated in Fig. 1. Measurements from CAP-2 and SOC collected in the marine boundary layer were normalized by the number of particles larger than 500 nm (N_{n500}; Fig. 1b), aerosol surface area (N_s; Fig. 1c) and aerosol volume (N_v; Fig. 1d) when simultaneous aerosol measurements were available. While aerosol surface area reduced the spread (in orders of magnitude) of observations the most, none of the normalizations applied here capture the variability in observed INP concentrations. This suggests parameterizations exclusively based on aerosol physical characteristics are only modestly useful in predicting marine INP concentrations, as also concluded by Tatzelt et al. (2022). To further investigate possible INP parameterization inputs, a Spearman's rank correlation analysis was performed between selected environmental variables, aerosol physical characteristics, and concentrations of INPs in binned temperature ranges; the results are shown in Fig. S6. No strong correlation was found between a single environmental or aerosol metric that applied for every temperature range of INPs, however, moderate but significant correlations ($p<0.05$) were found with both wind speed and aerosol surface area for temperatures colder than -21 °C. Tatzelt et al. (2022) performed a similar analysis between ACE INP concentrations and aerosol number and mass, but did not find any significant relationships between INP and aerosol measurements. However, it should be noted that they did not test for correlations with aerosol surface area, and they only had one INP measurement temperature colder than -21 °C.

SSA concentrations are known to increase with wind speed due to enhanced aerosol formation through wave breaking and bubble bursting (e.g. O'Dowd & de Leeuw, 2007). This relationship was also observed for INP concentrations in the MBL during SOC and CAP-2 (Fig. S7a). INP data used in Fig. S7 were limited to INPs active at temperatures <-27 °C to reduce the influence of temperature on the observed relationship, since freezing temperature exerts an outsized impact on measured INP concentrations. The wind speed range for the INP measurements shown in Fig. S7 was 4-23 m s^{-1}, which covers the majority of the observed range in the MBL during CAP-2 (0.1-28 m s^{-1}), though it should be noted measurements were limited to austral summer. Previous research into marine INPs has focused on organic and biological species (e.g. DeMott et al., 2016; McCluskey, Hill, Sultana, et al., 2018; McCluskey, Ovadnevaite, et al., 2018; Wilson et al., 2015), as soluble salts are not expected to contribute to heterogeneous ice nucleation in the immersion freezing mode, which is the most relevant nucleation mode for low and mixed-phase clouds (e.g. Kanji et al., 2017). Although limited to coastal measurements in the North Atlantic and North Pacific, Gantt et al. (2011) found the organic mass fraction of sea spray aerosol was inversely correlated with wind speed. Taken together, this would predict, if anything, negative correlations between normalized marine INP concentrations and wind speed. However, normalizing the INP concentrations by n500, aerosol surface area, or aerosol volume (Fig. S7b-d) did not remove the positive wind speed dependence, even though all three aerosol parameters are themselves positively correlated with wind speed (Moore et al., 2022). Figure 2 demonstrates that the positive correlation between INP concentration and wind speed extends across the full INP temperature range measured during SOC and CAP-2 and was similarly unaffected by normalization. Together, Fig. S7 and Fig. 2 suggest marine INP emissions are not strictly proportional to SSA production, but instead are enhanced at higher wind speeds through an unknown mechanism. This finding may help explain why parameterizing marine INPs based solely on aerosol physical parameters has not explained as much of the observed variability as for other INP types, particularly dust.

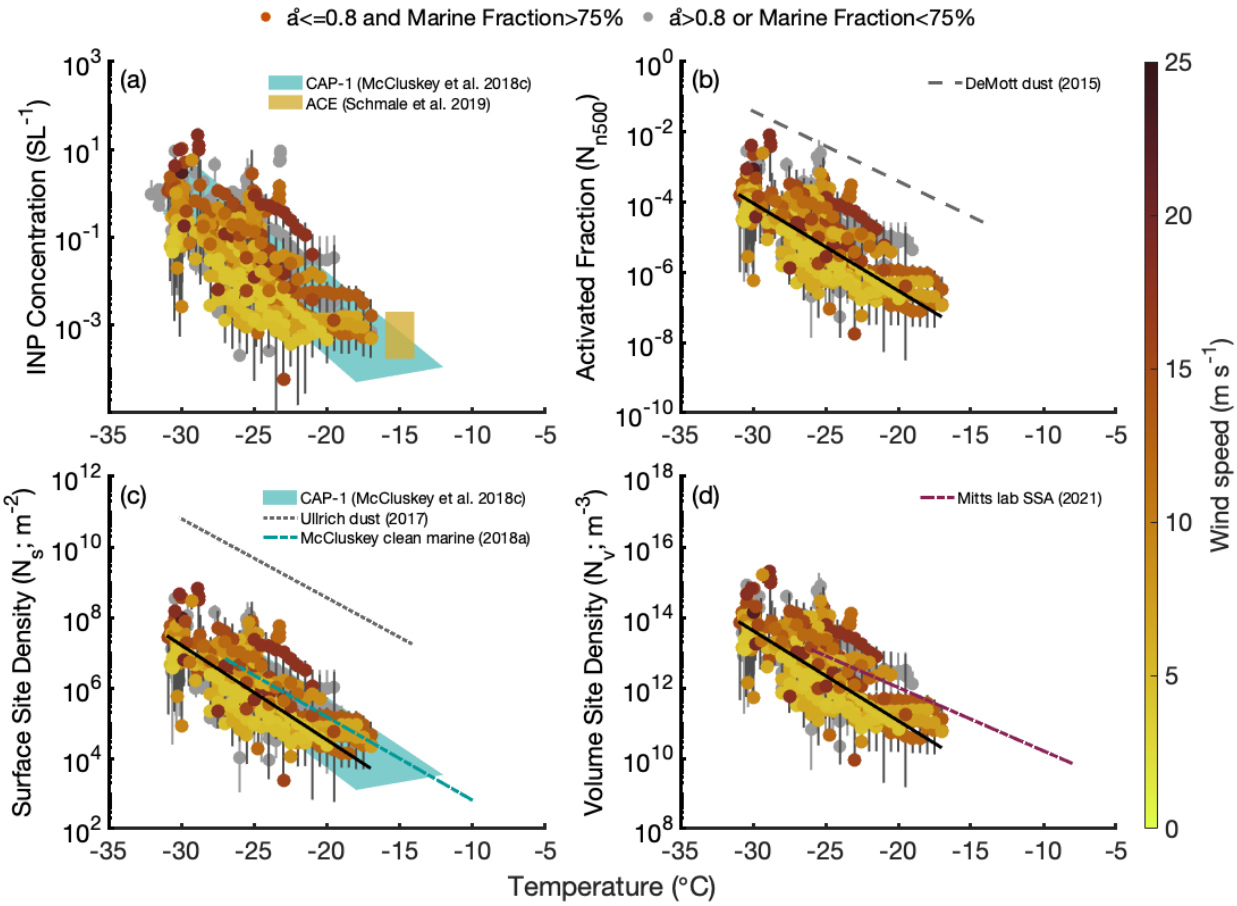

Figure 2. INP (a) concentration, (b) N_{n500}, (c) N_s and (d) N_v temperature spectra during SOC and CAP-2 in the MBL. All CFDC and filter measurements are shown as circles and colored by the average wind speed during each measurement period. The shading, parameterizations, best-fit lines, and marine aerosol classification are identical to Fig. 1.

Given the unexpected relationship found between INP concentrations and wind speed, we tested whether adding wind speed as an additional variable improved the marine INP parameterization developed by McCluskey, Ovadnevaite, et al. (2018). Following the approach of Niemand et al. (2012), N_s for Southern Ocean marine INPs was parameterized using an exponential relationship to activation temperature, with an additional exponential term for wind speed:

$$N_s(T, ws) = \exp(a \cdot T + b) + \exp(c \cdot ws + d) \#(2)$$

where N_s is the surface active site density (m^{-2}), T is temperature (°C), ws is wind speed (m s^{-1}), and a, b, c, and d are fit parameters. CAP-2 and SOC data used to derive the fit parameters were limited to the non-grey points shown in Fig. 2, namely, data collected within the marine boundary layer and with å<=0.8 and 5-day back trajectory ocean fraction >75% to isolate marine aerosol. The fit parameters were determined to be: a=-0.66±0.17, b=-3.11±5.11, c=0.51±0.09, and d=6.75±2.03 for this dataset. Modified normalized mean bias (B_n) was reduced from 0.54 to -0.18 by using the best-fit exponential to the SOC and CAP-2 marine boundary layer data instead of the parameterization derived from the North Atlantic (M18), as anticipated by the different

slopes seen in Fig. 1c. Using wind speed alone to predict N_s does a poor job reproducing the observations, with an increased bias B_n=1.07. Wind speed and temperature together performed the best, with a bias B_n=0.09, supporting its potential utility as a marine INP parameterization (Fig. 3).

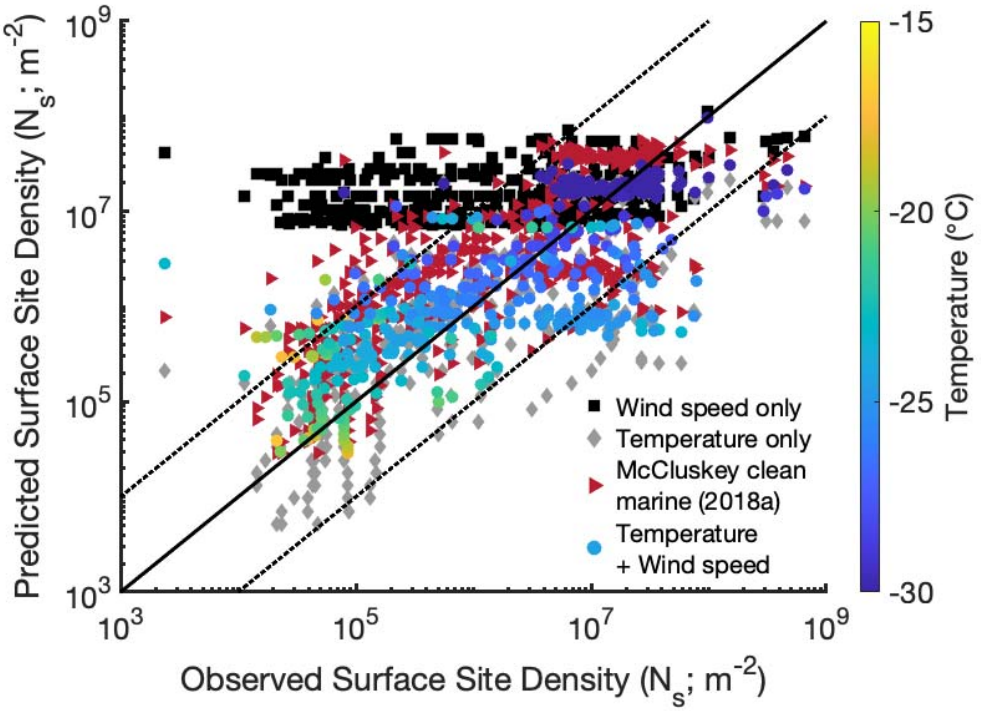

Figure 3. Predicted versus observed N_s during CAP-2 and SOC. Data shown are all from the MBL and are limited to observations with å<=0.8 and 5-day back trajectory ocean fraction >75% to isolate marine aerosol. Grey diamonds show a single-exponential fit using only temperature (B_n=-0.18), and black squares only wind speed (B_n=1.07). Non-grey circles show a 2-exponential fit (Eq. 2) to both wind speed and temperature and are colored by measurement temperature (B_n=0.09). Red triangles use the N_s parameterization from McCluskey, Ovadnevaite, et al. (2018) for clean marine air (B_n=0.54). The solid black line indicates a 1:1 relationship, and a factor of 10 deviation is shown by the dashed black lines.

3.3 Southern Ocean Marine INP size

As discussed in Sec. 2.3.3, both direct and indirect measurements of INP size were conducted during SOC and CAP-2, based on electron microscopy analysis of ice crystal residuals and INP concentration factors calculated during CAP-2. Measured INP concentration factors during CAP-2 had a maximum value of 37 and a median of 8.3, which are indicated in Fig. S4 by the grey shading and grey dashed line, respectively. For reference, the average INP concentration factor measured by Tobo et al. (2013) at a forested site in Colorado was 103, suggesting larger INPs were present than over the SO. Comparison with the aerosol concentrator calibration data implies the INPs measured by the CFDC during CAP-2 were dominated by particles <600 nm. CFDC ice crystal residuals collected during CAP-2 and SOC were as small as 0.1 μm; as previously discussed, the maximum size considered was 1.5 μm (Twohy et al., 2021). Ice crystal collections during CAP-2 utilized the aerosol concentrator, so the residual size distribution was corrected for

size-dependent enhancements using the calibration data shown in Fig. S4, as well as for size-dependent losses in the impactors upstream of the CFDC columns (Sec. 2.3.1), assuming residuals had the hygroscopicity and density of sea spray aerosols. The corrected median INP residual size was 0.18 μm, which agrees quite well with the 0.3-0.4 μm predicted from the median INP concentration factor measured during CAP-2 (Fig. S4), given both have large uncertainties. The smaller than expected sizes of Southern Ocean INPs is consistent with the lack of correlation observed by Tatzelt et al. (2022) between ACE INP concentrations and aerosol number or mass, as well as the generally poor or modest relationships found in this study (Sec 3.2; Fig. S6).

It should be noted that both analyses were limited to particles <1.5 μm due to the CFDC upstream impactors necessary to limit interferences from supermicron SSA in optical detection of ice crystals. Another potential complication is the use of measured concentration factors at relatively cold temperatures (<=-25 °C) to infer the median size of the overall marine INP population. Mason et al. (2016) found supermicron INPs dominated in most of their continental and coastal sites between -15 and -25 °C, and typically measured larger median sizes at warmer temperatures. While biological INPs can be as small as ~10 nm (e.g. Kanji et al., 2017; Pummer et al., 2015; Wilson et al., 2015), many bioaerosols are present in the coarse mode, and typically have warm onset temperatures if active as INPs (e.g. Hoose & Möhler, 2012; Kanji et al., 2017). Although the characteristic size distribution or mode size of ambient marine INPs is unknown, good correlation with aerosol surface area (DeMott et al., 2016; McCluskey, Ovadnevaite, et al., 2018), preferential emission in jet drops over film drops (Wang et al., 2017), and recent laboratory studies indicating supermicron marine INPs dominate below -14 °C (Mitts et al., 2021) had suggested the majority of marine INPs are >500 nm, if not larger. However, the excellent agreement between CFDC measurements, which sampled INPs <1.5 μm (CAP-2) or <2.5 μm (SOC), and the IS filter measurements, which captured larger particles, suggest the CFDCs were collecting most available INPs during CAP-2 and SOC (Fig. 1, 5). Future studies of size dependent INP concentrations in remote marine environments are needed to comprehensively assess the size distribution of marine INPs.

3.4 Altitude dependence

While modeling studies (Burrows et al., 2013; McCluskey et al., 2019, 2023; Vergara-Temprado et al., 2017) have provided insights into the expected vertical distribution of INPs in this region, SOCRATES measurements represent the first in situ observations in and above cloud to validate these results. Although temporally variable, the studies cited predict an increasing influence of mineral dust with height on average. Simulations of the CAPRICORN-1 field campaign (McCluskey et al., 2019) also suggested INP concentrations at -25 °C would decrease with height through the boundary layer and up to 3-4 km, then increase at higher altitudes. Some evidence supporting this structure is seen in Fig. 4a, which shows the CAP-2 and SOC INP concentrations as a function of altitude. A minimum in mean INP concentrations colder than -27 °C was seen between 2-4 km, with higher values in the MBL and around 6 km. The very limited observations above 6 km did not support the continued increase in INP concentrations with height predicted by McCluskey et al. (2019). When normalized by aerosol concentrations, N_{n500}, N_s and N_v were consistently higher above cloud and in the upper troposphere (>5000 m) than in the marine boundary layer, particularly N_{n500}. This finding is consistent with modeling results predicting different sources of INPs below and above-cloud. It also agrees with TEM measurements of single particles collected during SOCRATES flights, which found significantly

increased abundances of crustal and metal particles >0.5 μm above cloud versus in-cloud or in the MBL (Twohy et al., 2021). Above cloud and upper tropospheric N_{n500} were consistent with the DeMott et al. (2015) parameterization for dust (Fig. S8b), but N_s values were still 1-2 orders of magnitude lower than the Ullrich et al. (2017) dust parameterization (Fig. S8c). This discrepancy between the effectiveness of dust aerosol number- and surface area-based parameterizations has been reported previously for this region (McCluskey et al., 2019, 2023).

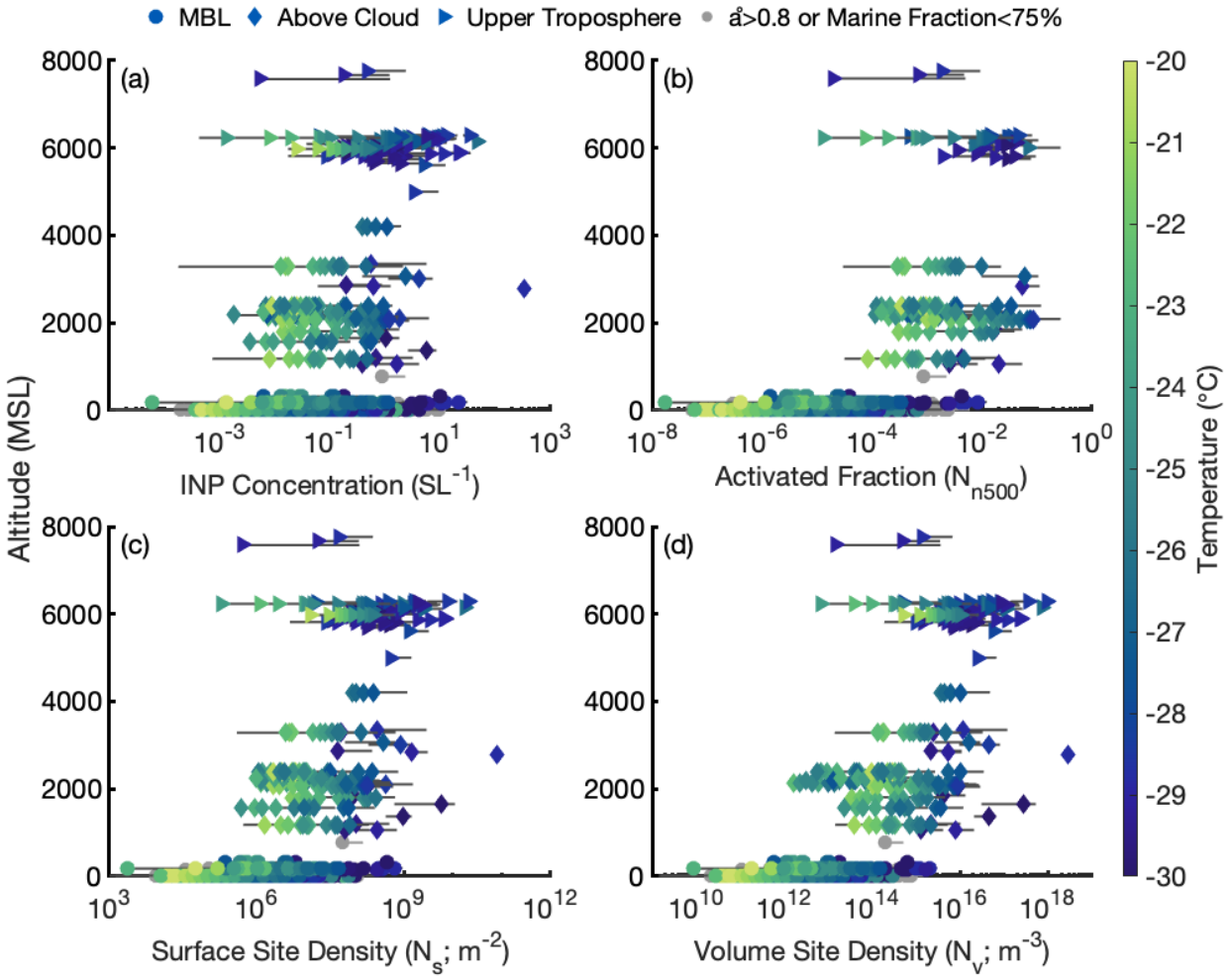

Figure 4. INP (a) concentration, (b) N_{n500}, (c) N_s and (d) N_v during SOC and CAP-2 as a function of altitude. Data in the MBL shown as circles, above cloud as diamonds, and upper troposphere (>5000 m) data as triangles. Non-grey symbols for the MBL data (circles) have å<=0.8 and 5-day back trajectory ocean fraction >75% to isolate marine aerosol; grey symbols do not meet at least one of these criteria. All symbols are colored by measurement temperature.

About half of the SOC research flights collected paired filter samples, with one in the MBL and one above cloud. Examples from RF05 (1/25-1/26/18) and RF14 (2/21-2/22/18) are shown in Fig. 5, along with SOC CFDC data separated into MBL and above-cloud measurements, in-cloud data on the CVI, and simulated CAM6 INP concentrations (Sec. 2.4) co-located with the SOC observations (McCluskey et al., 2023). When available, CAP-2 CFDC data during G-V overpasses of the RV *Investigator* are also shown for comparison. Due to the very different

speeds traveled by the ship and aircraft, measurements were counted as overpasses if they occurred within 30 minutes of each other, and the G-V was within 150 km of the RV *Investigator* during the measurement. Within uncertainty, the MBL and above-cloud measurements agreed for both flights shown here (Fig. 5a-b), as well as the in-cloud observations, which was typical for all of the flights with paired filters. When normalized by n500 (Fig. 5c-d) or aerosol surface area (Fig. 5e-f), some separation between the MBL and above-cloud measurements occurred for most flights with available data, with the largest separation for N_{n500}. Both the McCluskey, Ovadnevaite, et al. (2018) clean marine parameterization and the exponential fit derived in this study predict MBL N_s well on a flight-by-flight basis, while the dust-specific parameterization of Ullrich et al. (2017) uniformly overpredicts N_s, as seen throughout this work.

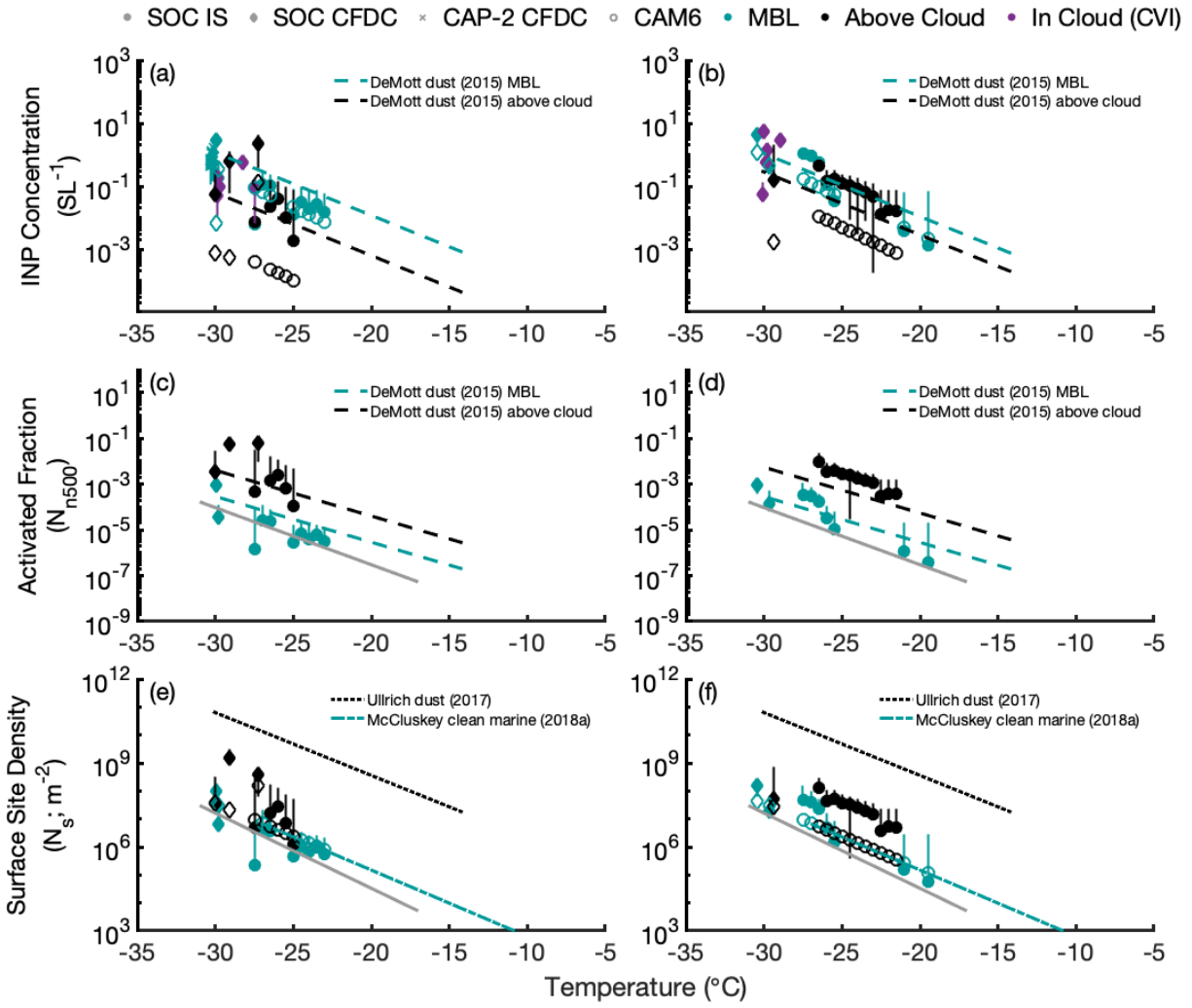

Figure 5. INP (a-b) concentration, (c-d) N_{n500}, and (e-f) N_s temperature spectra for SOCRATES flight RF05 (1/25-1/26/18) on the left and RF14 (2/21-2/22/18) on the right. Data in the MBL are shown as light blue symbols, and measurements above cloud in black. SOC filter measurements are circles, SOC CFDC are diamonds, simultaneous CAP-2 CFDC measurements are crosses (if available), and simulated CAM6 INP concentrations are open symbols (panels (a-b) and (e-f) only). If available, SOC CFDC observations in-cloud on the CVI are shown as purple diamonds

779 in panels (a-b). In panels (a-b) and (c-d), the blue and black dashed lines indicate the DeMott et
780 al. (2015) parameterization for dust based on n500 in the MBL and above cloud, respectively. In
781 (e-f), the black dotted line indicates the Ullrich et al. (2017) parameterization for dust N_s, and the
782 light blue dot-dash line shows the N_s parameterization from McCluskey, Ovadnevaite, et al.
783 (2018) for clean marine air. Solid grey lines in (c-d) and (e-f) indicate the best-fit exponential
784 functions to all the MBL data with non-grey symbols (Same as Figure 1).
785
786 Simulated total INP concentrations from CAM6 have variable agreement with the co-located
787 SOCRATES IS and CFDC measurements. As described in Sec. 2.4, CAM6 INP concentrations
788 are the sum of the sea spray INP contribution, based on simulated SSA surface area using M18,
789 and the dust INP contribution, using the number of simulated mineral dust particles larger than
790 500 nm and the DeMott et al. (2015) parameterization. Overall, the agreement is better for
791 observations in the MBL, while simulated above-cloud INP concentrations are biased low,
792 although there is significant variation among flights. The low bias of CAM6 above-cloud values
793 relative to observations is typically reduced when considering N_s (Fig. 5e-f) instead of INP
794 concentrations (Fig. 5a-b). This suggests that in addition to the surface level biases in aerosol
795 surface area, low biases in accumulation mode aerosol aloft, and large uncertainties in particle
796 composition aloft observed by McCluskey et al. (2023), there may also be a low bias in
797 simulated aerosol surface area above cloud, which is partially compensating for the
798 underestimation of INPs.
799 Fig. 5a-b and 5c-d include two lines indicating the DeMott et al. (2015) INP parameterization
800 for dust. Since D15 is specific to dust INPs but there were not continuous size-resolved
801 measurements of dust concentration, the required dust n500 inputs were estimated using STEM
802 measurements of aerosol composition averaged over SOCRATES (Sec. 2.2.3; Twohy et al.,
803 2021). The total n500 values measured during each SOC filter collection were scaled using the
804 average fraction of particles >0.5 μm that were categorized as crustal or metal types during SOC
805 (0.5 for above-cloud and 0.02 for MBL) to provide an estimate of dust n500. The dashed blue
806 and black lines in Fig. 5a-b indicate the dust INP concentrations predicted by D15. Fig. 5c-d
807 shows D15 normalized by the total n500 measured during each flight, to provide a fair
808 comparison to the SOC INP measurements, and thus represents the predicted N_{n500} if all the INPs
809 present were dust, but SSA contributes to n500. Excellent agreement was seen between both
810 parameterization estimates and their respective filters when normalized by total n500 (Fig. 5c-d).
811 More variable agreement was seen for absolute INP concentration estimates (Fig. 5a-b), though
812 most agree with the measurements within uncertainty. In addition to a low bias relative to the
813 SOC observations, CAM6 typically underpredicts INP concentrations relative to D15, especially
814 above cloud (Fig. 5a-b). Although not explored in McCluskey et al. (2023), this is consistent
815 with the underprediction of dust concentrations observed in E3SMv1 (Raman et al., 2023), as
816 well as an increasing contribution of dust to INP concentrations with height.
817 While this exercise does not provide direct evidence of the INP types present during SOC, it
818 does support the results shown in Fig. 4 and Fig. S8 that different types of INPs dominate at
819 different heights. Furthermore, if the average amount of dust measured by STEM during SOC
820 was present uniformly across the SO, D15-estimated dust INPs would be sufficient to account
821 for all or nearly all INPs measured, at all heights. This finding emphasizes the vast differences in
822 nucleation efficiency or site density between marine INPs and dust, and shows how even small
823 amounts of long-range transported dust can significantly influence SO cloud properties, as also
824 noted by McCluskey et al. (2023).

4 Summary

The Southern Ocean Cloud Radiation Aerosol Transport Experimental Study (SOCRATES) aircraft campaign, the second Clouds, Aerosols, Precipitation, Radiation and atmospherIc Composition Over the southeRN ocean (CAPRICORN-2) ship campaign, and affiliated projects in 2017-2018 were motivated by a lack of observations and understanding of cloud, aerosol, precipitation, and radiative processes and interactions in the Southern Ocean region (McFarquhar et al., 2021). This study presents measurements of INPs collected over the Southern Ocean in austral summer 2018, along with comparisons to CAM6 model simulations. Simultaneous aircraft and ship campaigns provided the first vertical distribution measurements of INPs in the region, including the first in situ observations in and above cloud. Our results confirm recent findings from the ACE (Schmale et al., 2019; Tatzelt et al., 2022; Welti et al., 2020) and CAPRICORN-1 (McCluskey, Hill, Humphries, et al., 2018) campaigns that INP concentrations in the SO marine boundary layer are lower at all latitudes than measurements made by Bigg (1973) in the late 1960s and early 1970s. The good agreement between CAP-2 CFDC data and SOC measurements during overpasses (Fig. 5) shows promise for future campaigns that might employ a similar multi-platform approach to understand vertical profiles of aerosols and INPs.

Modeling studies (Burrows et al., 2013; McCluskey et al., 2019, 2023; Vergara-Temprado et al., 2017) predicted marine INPs would dominate at low altitudes in the SO, with an increasing influence of mineral dust INPs with height. Paired MBL and above cloud measurements from SOC support this hypothesis (Fig. 5). Below- and above-cloud INP concentrations typically agree within uncertainty, however, higher ice nucleation efficiency was found above cloud, consistent with significantly enhanced dust concentrations observed in above cloud single-particle composition measurements (Twohy et al., 2021). The outsized impact dust INPs can have on SO cloud properties is also demonstrated in Fig. 5. Due to the vastly higher nucleation efficiency of mineral dust compared to marine INPs, dust INP concentrations predicted by the D15 parameterization were sufficient to account for almost all INPs measured, both in the MBL and at higher altitudes. However, this was based on bulk aerosol composition measurements and would require the average SOC dust n500 fraction to be present uniformly over the SO. As a result, the D15 predictions in Fig. 5 can only be interpreted as a broad verification of the relatively low nucleation efficiency of marine INPs, which still likely dominate primary ice nucleation in the SO MBL.

Both direct measurements of collected INP residuals and indirect inferences from enhancement factors measured using an aerosol concentrator suggest INPs in the MBL, at least those in the sub-2.5 μm range, are dominated by particles <500 nm. Small INP sizes are consistent with the minimal correlations observed between ACE INP concentrations and aerosol number or mass (Tatzelt et al., 2022), as well as the only modest relationships found in this study between INP concentrations and environmental or aerosol metrics (Fig. S6). However, both aerosol surface area and wind speed exhibited moderate correlations ($p<0.05$) for INP concentrations <-21 °C during SOC and CAP-2. Surprisingly, the correlation with wind speed remained after normalizing the INP concentrations by n500, aerosol surface area, or aerosol volume, suggesting marine INP emissions are not strictly proportional to SSA production (Fig. 2, Fig. S7). Following the approach of Niemand et al. (2012), a new parameterization for marine INPs is proposed, which includes wind speed in addition to activation temperature, and has reduced bias when compared to the existing parameterization of McCluskey et al. (2018). This parameterization captures the observed mean behavior well, but there is still significant

unexplained variability in INP concentrations remaining (Fig. 1, 3). One of the assumptions underlying the Niemand et al. (2012) and M18 approach is that the active site density is constant, or equivalently, the number of INPs per aerosol surface area is fixed. Marine INPs appear to violate this assumption, and wind speed, among other factors, plays a role in how INPs are distributed with aerosol surface area in the remote SO MBL.

Data Availability

All SOCRATES observational data is available from the NCAR/UCAR Earth Observing Laboratory (EOL) repository (https://data.eol.ucar.edu/master_lists/generated/socrates/). This includes navigation, aerosol, and microphysics measurements (UCAR/NCAR - Earth Observing Laboratory, 2019b), VCSEL RH data, (UCAR/NCAR - Earth Observing Laboratory, 2020), GNI observations (UCAR/NCAR - Earth Observing Laboratory, 2019a), CFDC data (DeMott et al., 2022), Ice Spectrometer measurements (DeMott & Hill, 2022), and aerosol composition results (Twohy & Toohey, 2020). CAPRICORN-2 CFDC (DeMott & Moore, 2022a), Ice Spectrometer (DeMott & Moore, 2022b), and INP composition (DeMott, 2021) measurements are also available on the SOCRATES EOL repository. SOCRATES CAM6 model simulations are archived online (McCluskey, 2022). All data and samples collected during the CAPRICORN-2 voyage are made publicly available in accordance with CSIRO Marine National Facility policy. Data from the voyage are available at https://doi.org/10.25919/5b71004e37a39 (CSIRO et al., 2018) following registration, and raw data are available by request (data-requests@marine.csiro.au). The time series of predicted exhaust influence on measurements during CAPRICORN-2 is available at https://data.csiro.au/collection/csiro%3A54903v2 (Humphries et al., 2022).

Acknowledgements

The authors thank the SOCRATES and CAPRICORN-2 science teams for the excellent planning, operations, and post-campaign discussions, especially PIs Jay Mace, Alain Protat, and Greg McFarquhar. The assistance and support of Cory Wolff and Pavel Romashkin, NCAR project managers for the SOCRATES project, as well as the G-V crew, are greatly appreciated. We especially thank Mike Reeves and Jorgen Jensen of NCAR for calibration, measurements, and analysis of GNI and UHSAS data from SOCRATES. We also thank the CSIRO Marine National Facility (MNF) for its support in the form of sea time on the RV *Investigator*, support personnel, scientific equipment, and data management during CAPRICORN-2. In particular, we wish to thank Ian McRobert (CSIRO Technical Services Officer) for assistance with the RV *Investigator's* electrical and data management systems during and after CAPRICORN-2, and to Ruhi Humphries (CSIRO Senior Research Scientist), Jason Ward (formerly CSIRO Senior Experimental Scientist) and Melita Keywood (CSIRO Research Director, Earth Systems) for their work maintaining aerosol equipment on board the RV *Investigator*. We thank Roy Geiss at the Colorado State University Electron Microscopy Lab for performing the STEM analytical measurements. The material in this article is based upon work supported by the National Center for Atmospheric Research, which is a major facility sponsored by the National Science Foundation under Cooperative Agreement 1852977. The data collected during SOCRATES used NSF's Lower Atmosphere Observing Facilities, which are managed and operated by NCAR's Earth Observing Laboratory. The authors gratefully acknowledge the NOAA Air Resources Laboratory (ARL) for the provision of the HYSPLIT transport and dispersion model (https://www.ready.noaa.gov) used in this publication. This work was primarily supported by the National Science Foundation (NSF)

through Grant AGS-1660486 (PJD, KAM, TCJH, SMK) and by the United States Department of Energy (DOE) through Grants DE-SC0018929 (PJD, TCJH) and DE-SC0021116 (PJD, TCJH, SMK). KAM acknowledges support by an NSF Graduate Research Fellowship under Grant 006784. CHT was supported by NSF AGS-1660605, DWT and BR by NSF AGS-1660537, and KJS by NSF AGS-1660374. CSM was supported by DOE Grant DE-SC0020098, with travel support from NSF AGS-1660486. Any opinions, findings, and conclusions or recommendations expressed in this material are those of the author(s) and do not necessarily reflect the views of the National Science Foundation.

References

Agresti, A., & Coull, B. A. (1998). Approximate Is Better than "Exact" for Interval Estimation of Binomial Proportions. *The American Statistician*, *52*(2), 119. https://doi.org/10.2307/2685469

Barry, K. R., Hill, T. C. J., Levin, E. J. T., Twohy, C. H., Moore, K. A., Weller, Z. D., et al. (2021). Observations of Ice Nucleating Particles in the Free Troposphere From Western US Wildfires. *Journal of Geophysical Research: Atmospheres*, *126*(3), e2020JD033752. https://doi.org/10.1029/2020JD033752

Bassett, G., & Koenker, R. (1978). Asymptotic Theory of Least Absolute Error Regression. *Journal of the American Statistical Association*, *73*(363), 618–622. https://doi.org/10.1080/01621459.1978.10480065

Bigg, E. K. (1973). Ice Nucleus Concentrations in Remote Areas. *Journal of the Atmospheric Sciences*, *30*(6), 1153–1157. https://doi.org/10.1175/1520-0469(1973)030<1153:INCIRA>2.0.CO;2

Bigg, E. K. (1990). Long-term trends in ice nucleus concentrations. *Atmospheric Research*, *25*(5), 409–415. https://doi.org/10.1016/0169-8095(90)90025-8

944 Bjordal, J., Storelvmo, T., Alterskjær, K., & Carlsen, T. (2020). Equilibrium climate sensitivity
945 above 5 °C plausible due to state-dependent cloud feedback. *Nature Geoscience*, *13*(11),
946 718–721. https://doi.org/10.1038/s41561-020-00649-1
947 Bodas-Salcedo, A., Williams, K. D., Ringer, M. A., Beau, I., Cole, J. N. S., Dufresne, J.-L., et al.
948 (2013). Origins of the Solar Radiation Biases over the Southern Ocean in CFMIP2
949 Models. *Journal of Climate*, *27*(1), 41–56. https://doi.org/10.1175/JCLI-D-13-00169.1
950 Bodas-Salcedo, A., Hill, P. G., Furtado, K., Williams, K. D., Field, P. R., Manners, J. C., et al.
951 (2016). Large Contribution of Supercooled Liquid Clouds to the Solar Radiation Budget
952 of the Southern Ocean. *Journal of Climate*, *29*(11), 4213–4228.
953 https://doi.org/10.1175/JCLI-D-15-0564.1
954 Bodas-Salcedo, A., Mulcahy, J. P., Andrews, T., Williams, K. D., Ringer, M. A., Field, P. R., &
955 Elsaesser, G. S. (2019). Strong Dependence of Atmospheric Feedbacks on Mixed-Phase
956 Microphysics and Aerosol-Cloud Interactions in HadGEM3. *Journal of Advances in*
957 *Modeling Earth Systems*, *11*(6), 1735–1758. https://doi.org/10.1029/2019MS001688
958 Brockmann, J. E. (2011). Aerosol Transport in Sampling Lines and Inlets. In *Aerosol*
959 *Measurement* (pp. 68–105). John Wiley & Sons, Ltd.
960 https://doi.org/10.1002/9781118001684.ch6
961 Bromwich, D. H., Nicolas, J. P., Hines, K. M., Kay, J. E., Key, E. L., Lazzara, M. A., et al.
962 (2012). Tropospheric clouds in Antarctica. *Reviews of Geophysics*, *50*(1).
963 https://doi.org/10.1029/2011RG000363
964 Burrows, S. M., Hoose, C., Pöschl, U., & Lawrence, M. G. (2013). Ice nuclei in marine air:
965 biogenic particles or dust? *Atmospheric Chemistry and Physics*, *13*(1), 245–267.
966 https://doi.org/10.5194/acp-13-245-2013

967 Chubb, T. H., Jensen, J. B., Siems, S. T., & Manton, M. J. (2013). In situ observations of
968 supercooled liquid clouds over the Southern Ocean during the HIAPER Pole-to-Pole
969 Observation campaigns. *Geophysical Research Letters*, *40*(19), 5280–5285.
970 https://doi.org/10.1002/grl.50986
971 Clegg, S. L., Brimblecombe, P., & Wexler, A. S. (1998). Thermodynamic Model of the System
972 H+−NH4+−Na+−SO42-−NO3-−Cl-−H2O at 298.15 K. *The Journal of Physical*
973 *Chemistry A*, *102*(12), 2155–2171. https://doi.org/10.1021/jp973043j
974 Clegg, S. L., Brimblecombe, P., & Wexler, A. S. (2021, May 30). E-AIM Home Page. Retrieved
975 October 7, 2021, from http://www.aim.env.uea.ac.uk/aim/aim.php
976 CSIRO, Marine National Facility, Rintoul, S. R., Protat, A., Bowie, A. R., Tilbrook, B., &
977 Bodrossy, L. (2018). RV Investigator Voyage IN2018_V01 End of Voyage (EOV)
978 Archive v4 [Data set]. CSIRO Data Collection. https://doi.org/10.25919/5b71004e37a39
979 DeMott, P. J. (2021). SOCRATES and CAPRICORN-2 Single Particle INP Composition via
980 STEM/EDS (Version 1.0) [Data set]. UCAR/NCAR - Earth Observing Laboratory.
981 https://doi.org/10.26023/THHB-X79P-A006
982 DeMott, P. J., & Hill, T. C. J. (2022). NSF/NCAR GV HIAPER Ice Spectrometer Data [Data
983 set]. UCAR/NCAR - Earth Observing Laboratory. https://doi.org/10.26023/TTHZ-474E-
984 B211
985 DeMott, P. J., & Moore, K. A. (2022a). CAPRICORN R/V Investigator Continuous Flow
986 Diffusion Chamber Measurements [Data set]. UCAR/NCAR - Earth Observing
987 Laboratory. https://doi.org/10.26023/K5NQ-P9AB-KH06

988 DeMott, P. J., & Moore, K. A. (2022b). CAPRICORN R/V Investigator Ice Spectrometer
989 Measurements [Data set]. UCAR/NCAR - Earth Observing Laboratory.
990 https://doi.org/10.26023/RTYY-YDBS-6W06
991 DeMott, P. J., Prenni, A. J., Liu, X., Kreidenweis, S. M., Petters, M. D., Twohy, C. H., et al.
992 (2010). Predicting global atmospheric ice nuclei distributions and their impacts on
993 climate. *Proceedings of the National Academy of Sciences*, *107*(25), 11217–11222.
994 https://doi.org/10.1073/pnas.0910818107
995 DeMott, P. J., Prenni, A. J., McMeeking, G. R., Sullivan, R. C., Petters, M. D., Tobo, Y., et al.
996 (2015). Integrating laboratory and field data to quantify the immersion freezing ice
997 nucleation activity of mineral dust particles. *Atmospheric Chemistry and Physics*, *15*(1),
998 393–409. https://doi.org/10.5194/acp-15-393-2015
999 DeMott, P. J., Hill, T. C. J., McCluskey, C. S., Prather, K. A., Collins, D. B., Sullivan, R. C., et
1000 al. (2016). Sea spray aerosol as a unique source of ice nucleating particles. *Proceedings*
1001 *of the National Academy of Sciences*, *113*(21), 5797–5803.
1002 https://doi.org/10.1073/pnas.1514034112
1003 DeMott, P. J., Hill, T. C., Marchand, R., & Alexander, S. (2018). *Macquarie Island Cloud and*
1004 *Radiation Experiment (MICRE) Ice Nucleating Particle Measurements Field Campaign*
1005 *Report* (No. DOE/SC-ARM-18-030). ARM user facility, Pacific Northwest National
1006 Laboratory, Richland, WA. Retrieved from https://www.osti.gov/biblio/1489359
1007 DeMott, P. J., Hill, T. C., & McFarquhar, G. (2018). *Measurements of Aerosols, Radiation, and*
1008 *Clouds over the Southern Ocean (MARCUS) Ice Nucleating Particle Measurements Field*
1009 *Campaign Report* (No. DOE/SC-ARM-18-031). ARM user facility, Pacific Northwest

1010 National Laboratory, Richland, WA. Retrieved from
1011 https://www.osti.gov/biblio/1489372
1012 DeMott, P. J., Möhler, O., Cziczo, D. J., Hiranuma, N., Petters, M. D., Petters, S. S., et al. (2018).
1013 The Fifth International Workshop on Ice Nucleation phase 2 (FIN-02): laboratory
1014 intercomparison of ice nucleation measurements. *Atmospheric Measurement Techniques*,
1015 *11*(11), 6231–6257. https://doi.org/10.5194/amt-11-6231-2018
1016 DeMott, P. J., Moore, K. A., & McCluskey, C. S. (2022). SOCRATES: NSF/NCAR GV
1017 HIAPER Continuous Flow Diffusion Chamber Measurements [Data set]. UCAR/NCAR -
1018 Earth Observing Laboratory. https://doi.org/10.26023/P469-803K-WP0W
1019 Frey, W. R., & Kay, J. E. (2017). The influence of extratropical cloud phase and amount
1020 feedbacks on climate sensitivity. *Climate Dynamics*, *50*(7), 3097–3116.
1021 https://doi.org/10.1007/s00382-017-3796-5
1022 Gantt, B., Meskhidze, N., Facchini, M. C., Rinaldi, M., Ceburnis, D., & O'Dowd, C. D. (2011).
1023 Wind speed dependent size-resolved parameterization for the organic mass fraction of sea
1024 spray aerosol. *Atmospheric Chemistry and Physics*, *11*(16), 8777–8790.
1025 https://doi.org/10.5194/acp-11-8777-2011
1026 Gettelman, A., Mills, M. J., Kinnison, D. E., Garcia, R. R., Smith, A. K., Marsh, D. R., et al.
1027 (2019). The Whole Atmosphere Community Climate Model Version 6 (WACCM6).
1028 *Journal of Geophysical Research: Atmospheres*, *124*(23), 12380–12403.
1029 https://doi.org/10.1029/2019JD030943
1030 Gettelman, A., Bardeen, C. G., McCluskey, C. S., Järvinen, E., Stith, J., Bretherton, C., et al.
1031 (2020). Simulating Observations of Southern Ocean Clouds and Implications for Climate.

Journal of Geophysical Research: Atmospheres, *125*(21), e2020JD032619. https://doi.org/10.1029/2020JD032619

Ginoux, P., Prospero, J. M., Gill, T. E., Hsu, N. C., & Zhao, M. (2012). Global-scale attribution of anthropogenic and natural dust sources and their emission rates based on MODIS Deep Blue aerosol products. *Reviews of Geophysics*, *50*(3). https://doi.org/10.1029/2012RG000388

Hiranuma, N., Augustin-Bauditz, S., Bingemer, H., Budke, C., Curtius, J., Danielczok, A., et al. (2015). A comprehensive laboratory study on the immersion freezing behavior of illite NX particles: a comparison of 17 ice nucleation measurement techniques. *Atmospheric Chemistry and Physics*, *15*(5), 2489–2518. https://doi.org/10.5194/acp-15-2489-2015

Hoose, C., & Möhler, O. (2012). Heterogeneous ice nucleation on atmospheric aerosols: a review of results from laboratory experiments. *Atmospheric Chemistry and Physics*, *12*(20), 9817–9854. https://doi.org/10.5194/acp-12-9817-2012

Humphries, R. S., McRobert, I. M., Ponsonby, W. A., Ward, J. P., Keywood, M. D., Loh, Z. M., et al. (2019). Identification of platform exhaust on the RV *Investigator*. *Atmospheric Measurement Techniques*, *12*(6), 3019–3038. https://doi.org/10.5194/amt-12-3019-2019

Humphries, R. S., Keywood, M. D., Gribben, S., McRobert, I. M., Ward, J. P., Selleck, P., et al. (2021). Southern Ocean latitudinal gradients of Cloud Condensation Nuclei. *Atmospheric Chemistry and Physics Discussions*, 1–35. https://doi.org/10.5194/acp-2020-1246

Humphries, R. S., McRobert, I. M., Ponsonby, W. A., Ward, J. P., Keywood, M. D., Loh, Z. M., et al. (2022). Exhaust identification data from IN2018_V01 (CAPRICORN2) [Data set]. https://doi.org/10.25919/f8s8-cy20

1054 Irish, V. E., Hanna, S. J., Willis, M. D., China, S., Thomas, J. L., Wentzell, J. J. B., et al. (2019).
1055 Ice nucleating particles in the marine boundary layer in the Canadian Arctic during
1056 summer 2014. *Atmospheric Chemistry and Physics*, *19*(2), 1027–1039.
1057 https://doi.org/10.5194/acp-19-1027-2019
1058 Järvinen, E., McCluskey, C. S., Waitz, F., Schnaiter, M., Bansemer, A., Bardeen, C. G., et al.
1059 (2022). Evidence for Secondary Ice Production in Southern Ocean Maritime Boundary
1060 Layer Clouds. *Journal of Geophysical Research: Atmospheres*, *127*(16), e2021JD036411.
1061 https://doi.org/10.1029/2021JD036411
1062 Jensen, J. B., Beaton, S. P., Stith, J. L., Schwenz, K., Colón-Robles, M., Rauber, R. M., & Gras,
1063 J. (2020). The Giant Nucleus Impactor (GNI)—A System for the Impaction and
1064 Automated Optical Sizing of Giant Aerosol Particles with Emphasis on Sea Salt. Part I:
1065 Basic Instrument and Algorithms. *Journal of Atmospheric and Oceanic Technology*,
1066 *37*(9), 1551–1569. https://doi.org/10.1175/JTECH-D-19-0109.1
1067 Kanji, Z. A., Ladino, L. A., Wex, H., Boose, Y., Burkert-Kohn, M., Cziczo, D. J., & Krämer, M.
1068 (2017). Overview of Ice Nucleating Particles. *Meteorological Monographs*, *58*, 1.1-1.33.
1069 https://doi.org/10.1175/AMSMONOGRAPHS-D-16-0006.1
1070 Kay, J. E., Bourdages, L., Miller, N. B., Morrison, A., Yettella, V., Chepfer, H., & Eaton, B.
1071 (2016). Evaluating and improving cloud phase in the Community Atmosphere Model
1072 version 5 using spaceborne lidar observations. *Journal of Geophysical Research:*
1073 *Atmospheres*, *121*(8), 4162–4176. https://doi.org/10.1002/2015JD024699
1074 Kay, J. E., Wall, C., Yettella, V., Medeiros, B., Hannay, C., Caldwell, P., & Bitz, C. (2016).
1075 Global Climate Impacts of Fixing the Southern Ocean Shortwave Radiation Bias in the

1076 Community Earth System Model (CESM). *Journal of Climate*, *29*(12), 4617–4636.
1077 https://doi.org/10.1175/JCLI-D-15-0358.1
1078 Kremser, S., Harvey, M., Kuma, P., Hartery, S., Saint-Macary, A., McGregor, J., et al. (2021).
1079 Southern Ocean cloud and aerosol data: a compilation of measurements from the 2018
1080 Southern Ocean Ross Sea Marine Ecosystems and Environment voyage. *Earth System*
1081 *Science Data*, *13*(7), 3115–3153. https://doi.org/10.5194/essd-13-3115-2021
1082 Krishnamoorthy, K., & Lee, M. (2012). New approximate confidence intervals for the difference
1083 between two Poisson means and comparison. *Journal of Statistical Computation and*
1084 *Simulation*, *83*(12), 2232–2243. https://doi.org/10.1080/00949655.2012.686616
1085 Lance, S., Brock, C. A., Rogers, D., & Gordon, J. A. (2010). Water droplet calibration of the
1086 Cloud Droplet Probe (CDP) and in-flight performance in liquid, ice and mixed-phase
1087 clouds during ARCPAC. *Atmospheric Measurement Techniques*, *3*(6), 1683–1706.
1088 https://doi.org/10.5194/amt-3-1683-2010
1089 Li, G., Wieder, J., Pasquier, J. T., Henneberger, J., & Kanji, Z. A. (2022). Predicting atmospheric
1090 background number concentration of ice-nucleating particles in the Arctic. *Atmospheric*
1091 *Chemistry and Physics*, *22*(21), 14441–14454. https://doi.org/10.5194/acp-22-14441-
1092 2022
1093 Liu, X., Ma, P.-L., Wang, H., Tilmes, S., Singh, B., Easter, R. C., et al. (2016). Description and
1094 evaluation of a new four-mode version of the Modal Aerosol Module (MAM4) within
1095 version 5.3 of the Community Atmosphere Model. *Geoscientific Model Development*,
1096 *9*(2), 505–522. https://doi.org/10.5194/gmd-9-505-2016
1097 Mace, G. G., Protat, A., Humphries, R. S., Alexander, S. P., McRobert, I. M., Ward, J., et al.
1098 (2020). Southern Ocean Cloud Properties Derived from CAPRICORN and MARCUS

1099 Data. *Journal of Geophysical Research: Atmospheres*, e2020JD033368.
1100 https://doi.org/10.1029/2020JD033368
1101 Maring, H., Savoie, D. L., Izaguirre, M. A., Custals, L., & Reid, J. S. (2003). Mineral dust
1102 aerosol size distribution change during atmospheric transport. *Journal of Geophysical*
1103 *Research: Atmospheres*, *108*(D19). https://doi.org/10.1029/2002JD002536
1104 Mårtensson, E. M., Nilsson, E. D., de Leeuw, G., Cohen, L. H., & Hansson, H.-C. (2003).
1105 Laboratory simulations and parameterization of the primary marine aerosol production.
1106 *Journal of Geophysical Research: Atmospheres*, *108*(D9).
1107 https://doi.org/10.1029/2002JD002263
1108 Mason, R. H., Si, M., Chou, C., Irish, V. E., Dickie, R., Elizondo, P., et al. (2016). Size-resolved
1109 measurements of ice-nucleating particles at six locations in North America and one in
1110 Europe. *Atmospheric Chemistry and Physics*, *16*(3), 1637–1651.
1111 https://doi.org/10.5194/acp-16-1637-2016
1112 McCluskey, C. S. (2022). Archived Model Output for "Simulating Observations of Southern
1113 Ocean Clouds and Implications for Climate" (Version 1) [Data set]. Zenodo.
1114 https://doi.org/10.5281/zenodo.6463951
1115 McCluskey, C. S., DeMott, P. J., Prenni, A. J., Levin, E. J. T., McMeeking, G. R., Sullivan, A. P.,
1116 et al. (2014). Characteristics of atmospheric ice nucleating particles associated with
1117 biomass burning in the US: Prescribed burns and wildfires. *Journal of Geophysical*
1118 *Research: Atmospheres*, *119*(17), 10458–10470. https://doi.org/10.1002/2014JD021980
1119 McCluskey, C. S., Hill, T. C. J., Sultana, C. M., Laskina, O., Trueblood, J., Santander, M. V., et
1120 al. (2018). A Mesocosm Double Feature: Insights into the Chemical Makeup of Marine

Ice Nucleating Particles. *Journal of the Atmospheric Sciences*, *75*(7), 2405–2423. https://doi.org/10.1175/JAS-D-17-0155.1

McCluskey, C. S., Ovadnevaite, J., Rinaldi, M., Atkinson, J., Belosi, F., Ceburnis, D., et al. (2018). Marine and Terrestrial Organic Ice-Nucleating Particles in Pristine Marine to Continentally Influenced Northeast Atlantic Air Masses. *Journal of Geophysical Research: Atmospheres*, *123*(11), 6196–6212. https://doi.org/10.1029/2017JD028033

McCluskey, C. S., Hill, T. C. J., Humphries, R. S., Rauker, A. M., Moreau, S., Strutton, P. G., et al. (2018). Observations of Ice Nucleating Particles Over Southern Ocean Waters. *Geophysical Research Letters*, *45*(21), 11,989-11,997. https://doi.org/10.1029/2018GL079981

McCluskey, C. S., DeMott, P. J., Ma, P.-L., & Burrows, S. M. (2019). Numerical Representations of Marine Ice-Nucleating Particles in Remote Marine Environments Evaluated Against Observations. *Geophysical Research Letters*, *46*(13), 7838–7847. https://doi.org/10.1029/2018GL081861

McCluskey, C. S., Gettelman, A., Bardeen, C. G., DeMott, P. J., Moore, K. A., Kreidenweis, S. M., et al. (2023). Simulating Southern Ocean Aerosol and Ice Nucleating Particles in the Community Earth System Model Version 2. *Journal of Geophysical Research: Atmospheres*, *n/a*(n/a), e2022JD036955. https://doi.org/10.1029/2022JD036955

McFarquhar, G. M., Bretherton, C. S., Marchand, R., Protat, A., DeMott, P. J., Alexander, S. P., et al. (2021). Observations of Clouds, Aerosols, Precipitation, and Surface Radiation over the Southern Ocean: An Overview of CAPRICORN, MARCUS, MICRE, and SOCRATES. *Bulletin of the American Meteorological Society*, *102*(4), E894–E928. https://doi.org/10.1175/BAMS-D-20-0132.1

1144 Mitts, B. A., Wang, X., Lucero, D. D., Beall, C. M., Deane, G. B., DeMott, P. J., & Prather, K. A.
1145 (2021). Importance of Supermicron Ice Nucleating Particles in Nascent Sea Spray.
1146 *Geophysical Research Letters*, *48*(3), e2020GL089633.
1147 https://doi.org/10.1029/2020GL089633
1148 Miyakawa, T., Taketani, F., Tobo, Y., Matsumoto, K., Yoshizue, M., Takigawa, M., & Kanaya,
1149 Y. (2023). Measurements of Aerosol Particle Size Distributions and INPs Over the
1150 Southern Ocean in the Late Austral Summer of 2017 on Board the R/V Mirai: Importance
1151 of the Marine Boundary Layer Structure. *Earth and Space Science*, *10*(3),
1152 e2022EA002736. https://doi.org/10.1029/2022EA002736
1153 Modini, R. L., Frossard, A. A., Ahlm, L., Russell, L. M., Corrigan, C. E., Roberts, G. C., et al.
1154 (2015). Primary marine aerosol-cloud interactions off the coast of California. *Journal of*
1155 *Geophysical Research: Atmospheres*, *120*(9), 4282–4303.
1156 https://doi.org/10.1002/2014JD022963
1157 Monahan, E. C., & Muircheartaigh, I. (1980). Optimal Power-Law Description of Oceanic
1158 Whitecap Coverage Dependence on Wind Speed. *Journal of Physical Oceanography*,
1159 *10*(12), 2094–2099. https://doi.org/10.1175/1520-
1160 0485(1980)010<2094:OPLDOO>2.0.CO;2
1161 Monahan, E. C., Spiel, D. E., & Davidson, K. L. (1986). A Model of Marine Aerosol Generation
1162 Via Whitecaps and Wave Disruption. In E. C. Monahan & G. M. Niocaill (Eds.), *Oceanic*
1163 *Whitecaps: And Their Role in Air-Sea Exchange Processes* (pp. 167–174). Dordrecht:
1164 Springer Netherlands. https://doi.org/10.1007/978-94-009-4668-2_16
1165 Moore, K. A. (2020). *Constraining marine ice nucleating particle parameterizations in*
1166 *atmospheric models using observations from the Southern Ocean* (MS Thesis). Colorado

1167 State University, https://mountainscholar.org/handle/10217/208435. Retrieved from
1168 https://mountainscholar.org/handle/10217/208435
1169 Moore, K. A., Alexander, S. P., Humphries, R. S., Jensen, J., Protat, A., Reeves, J. M., et al.
1170 (2022). Estimation of Sea Spray Aerosol Surface Area Over the Southern Ocean Using
1171 Scattering Measurements. *Journal of Geophysical Research: Atmospheres*, *127*(22),
1172 e2022JD037009. https://doi.org/10.1029/2022JD037009
1173 Morrison, A. E., Siems, S. T., & Manton, M. J. (2011). A Three-Year Climatology of Cloud-Top
1174 Phase over the Southern Ocean and North Pacific. *Journal of Climate*, *24*(9), 2405–2418.
1175 https://doi.org/10.1175/2010JCLI3842.1
1176 Naud, C. M., Booth, J. F., & Genio, A. D. D. (2014). Evaluation of ERA-Interim and MERRA
1177 Cloudiness in the Southern Ocean. *Journal of Climate*, *27*(5), 2109–2124.
1178 https://doi.org/10.1175/JCLI-D-13-00432.1
1179 Niemand, M., Möhler, O., Vogel, B., Vogel, H., Hoose, C., Connolly, P., et al. (2012). A
1180 Particle-Surface-Area-Based Parameterization of Immersion Freezing on Desert Dust
1181 Particles. *Journal of the Atmospheric Sciences*, *69*(10), 3077–3092.
1182 https://doi.org/10.1175/JAS-D-11-0249.1
1183 Noone, K. J., Ogren, J. A., Heintzenberg, J., Charlson, R. J., & Covert, D. S. (1988). Design and
1184 Calibration of a Counterflow Virtual Impactor for Sampling of Atmospheric Fog and
1185 Cloud Droplets. *Aerosol Science and Technology*, *8*(3), 235–244.
1186 https://doi.org/10.1080/02786828808959186
1187 O'Dowd, C. D., & de Leeuw, G. (2007). Marine aerosol production: a review of the current
1188 knowledge. *Philosophical Transactions of the Royal Society A: Mathematical, Physical*
1189 *and Engineering Sciences*, *365*(1856), 1753–1774. https://doi.org/10.1098/rsta.2007.2043

1190 Pruppacher, H. R., & Klett, J. D. (2010). *Microphysics of Clouds and Precipitation* (2nd ed.).
1191 Springer Netherlands. https://doi.org/10.1007/978-0-306-48100-0
1192 Pummer, B. G., Budke, C., Augustin-Bauditz, S., Niedermeier, D., Felgitsch, L., Kampf, C. J., et
1193 al. (2015). Ice nucleation by water-soluble macromolecules. *Atmospheric Chemistry and*
1194 *Physics*, *15*(8), 4077–4091. https://doi.org/10.5194/acp-15-4077-2015
1195 Quinn, P. K., Coffman, D. J., Johnson, J. E., Upchurch, L. M., & Bates, T. S. (2017). Small
1196 fraction of marine cloud condensation nuclei made up of sea spray aerosol. *Nature*
1197 *Geoscience*, *10*(9), 674–679. https://doi.org/10.1038/ngeo3003
1198 Raman, A., Hill, T., DeMott, P. J., Singh, B., Zhang, K., Ma, P.-L., et al. (2023). Long-term
1199 variability in immersion-mode marine ice-nucleating particles from climate model
1200 simulations and observations. *Atmospheric Chemistry and Physics*, *23*(10), 5735–5762.
1201 https://doi.org/10.5194/acp-23-5735-2023
1202 Rogers, D. C. (1988). Development of a continuous flow thermal gradient diffusion chamber for
1203 ice nucleation studies. *Atmospheric Research*, *22*(2), 149–181.
1204 https://doi.org/10.1016/0169-8095(88)90005-1
1205 Rogers, D. C., DeMott, P. J., Kreidenweis, S. M., & Chen, Y. (2001). A Continuous-Flow
1206 Diffusion Chamber for Airborne Measurements of Ice Nuclei. *Journal of Atmospheric*
1207 *and Oceanic Technology*, *18*, 17.
1208 Rolph, G., Stein, A., & Stunder, B. (2017). Real-time Environmental Applications and Display
1209 sYstem: READY. *Environmental Modelling & Software*, *95*, 210–228.
1210 https://doi.org/10.1016/j.envsoft.2017.06.025
1211 Rosenfeld, D., Chemke, R., DeMott, P. J., Sullivan, R. C., Rasmussen, R., McDonough, F., et al.
1212 (2013). The common occurrence of highly supercooled drizzle and rain near the coastal

regions of the western United States. *Journal of Geophysical Research: Atmospheres*, *118*(17), 9819–9833. https://doi.org/10.1002/jgrd.50529

Rosinski, J., Haagenson, P. L., Nagamoto, C. T., & Parungo, F. (1987). Nature of ice-forming nuclei in marine air masses. *Journal of Aerosol Science*, *18*(3), 291–309. https://doi.org/10.1016/0021-8502(87)90024-3

Sanchez, K. J., Zhang, B., Liu, H., Saliba, G., Chen, C.-L., Lewis, S. L., et al. (2021). Linking marine phytoplankton emissions, meteorological processes, and downwind particle properties with FLEXPART. *Atmospheric Chemistry and Physics*, *21*(2), 831–851. https://doi.org/10.5194/acp-21-831-2021

Sanchez, K. J., Roberts, G. C., Saliba, G., Russell, L. M., Twohy, C., Reeves, J. M., et al. (2021). Measurement report: Cloud processes and the transport of biological emissions affect southern ocean particle and cloud condensation nuclei concentrations. *Atmospheric Chemistry and Physics*, *21*(5), 3427–3446. https://doi.org/10.5194/acp-21-3427-2021

Schill, G. P., Jathar, S. H., Kodros, J. K., Levin, E. J. T., Galang, A. M., Friedman, B., et al. (2016). Ice-nucleating particle emissions from photochemically aged diesel and biodiesel exhaust. *Geophysical Research Letters*, *43*(10), 5524–5531. https://doi.org/10.1002/2016GL069529

Schmale, J., Baccarini, A., Thurnherr, I., Henning, S., Efraim, A., Regayre, L., et al. (2019). Overview of the Antarctic Circumnavigation Expedition: Study of Preindustrial-like Aerosols and Their Climate Effects (ACE-SPACE). *Bulletin of the American Meteorological Society*, *100*(11), 2260–2283. https://doi.org/10.1175/BAMS-D-18-0187.1

1235 Stein, A. F., Draxler, R. R., Rolph, G. D., Stunder, B. J. B., Cohen, M. D., & Ngan, F. (2015).
1236 NOAA's HYSPLIT Atmospheric Transport and Dispersion Modeling System. *Bulletin of*
1237 *the American Meteorological Society*, *96*(12), 2059–2077.
1238 https://doi.org/10.1175/BAMS-D-14-00110.1
1239 Stith, J. L., Ramanathan, V., Cooper, W. A., Roberts, G. C., DeMott, P. J., Carmichael, G., et al.
1240 (2009). An overview of aircraft observations from the Pacific Dust Experiment campaign.
1241 *Journal of Geophysical Research: Atmospheres*, *114*(D5).
1242 https://doi.org/10.1029/2008JD010924
1243 Tan, I., Storelvmo, T., & Zelinka, M. D. (2016). Observational constraints on mixed-phase
1244 clouds imply higher climate sensitivity. *Science*, *352*(6282), 224–227.
1245 https://doi.org/10.1126/science.aad5300
1246 Tang, I. N., Tridico, A. C., & Fung, K. H. (1997). Thermodynamic and optical properties of sea
1247 salt aerosols. *Journal of Geophysical Research: Atmospheres*, *102*(D19), 23269–23275.
1248 https://doi.org/10.1029/97JD01806
1249 Tatzelt, C., Henning, S., Welti, A., Baccarini, A., Hartmann, M., Gysel-Beer, M., et al. (2022).
1250 Circum-Antarctic abundance and properties of CCN and INPs. *Atmospheric Chemistry*
1251 *and Physics*, *22*(14), 9721–9745. https://doi.org/10.5194/acp-22-9721-2022
1252 Testa, B., Hill, T. C. J., Marsden, N. A., Barry, K. R., Hume, C. C., Bian, Q., et al. (2021). Ice
1253 Nucleating Particle Connections to Regional Argentinian Land Surface Emissions and
1254 Weather During the Cloud, Aerosol, and Complex Terrain Interactions Experiment.
1255 *Journal of Geophysical Research: Atmospheres*, *126*(23), e2021JD035186.
1256 https://doi.org/10.1029/2021JD035186

1257 Tobo, Y., Prenni, A. J., DeMott, P. J., Huffman, J. A., McCluskey, C. S., Tian, G., et al. (2013).
1258 Biological aerosol particles as a key determinant of ice nuclei populations in a forest
1259 ecosystem. *Journal of Geophysical Research: Atmospheres*, *118*(17), 10,100-10,110.
1260 https://doi.org/10.1002/jgrd.50801
1261 Twohy, C. H., & Toohey, D. W. (2020). Single Particle Composition via STEM/EDS (Version
1262 1.0) [Data set]. UCAR/NCAR - Earth Observing Laboratory.
1263 https://doi.org/10.26023/55HP-PSEF-WC07
1264 Twohy, C. H., DeMott, P. J., Pratt, K. A., Subramanian, R., Kok, G. L., Murphy, S. M., et al.
1265 (2010). Relationships of Biomass-Burning Aerosols to Ice in Orographic Wave Clouds.
1266 *Journal of the Atmospheric Sciences*, *67*(8), 2437–2450.
1267 https://doi.org/10.1175/2010JAS3310.1
1268 Twohy, C. H., McMeeking, G. R., DeMott, P. J., McCluskey, C. S., Hill, T. C. J., Burrows, S.
1269 M., et al. (2016). Abundance of fluorescent biological aerosol particles at temperatures
1270 conducive to the formation of mixed-phase and cirrus clouds. *Atmospheric Chemistry and*
1271 *Physics*, *16*(13), 8205–8225. https://doi.org/10.5194/acp-16-8205-2016
1272 Twohy, C. H., DeMott, P. J., Russell, L. M., Toohey, D. W., Rainwater, B., Geiss, R., et al.
1273 (2021). Cloud-Nucleating Particles Over the Southern Ocean in a Changing Climate.
1274 *Earth's Future*, *9*(3), e2020EF001673. https://doi.org/10.1029/2020EF001673
1275 UCAR/NCAR - Earth Observing Laboratory. (2005). *NSF/NCAR GV HIAPER Aircraft*.
1276 https://doi.org/10.5065/D6DR2SJP.
1277 UCAR/NCAR - Earth Observing Laboratory. (2019a). SOCRATES: Giant Cloud Condensation
1278 Nuclei (CCN) Impactor Data [Data set]. UCAR/NCAR - Earth Observing Laboratory.
1279 https://data.eol.ucar.edu/dataset/552.048

1280 UCAR/NCAR - Earth Observing Laboratory. (2019b). UCAR/NCAR – Earth Observing
1281 Laboratory: Low Rate (LRT -1 sps) Navigation, State Parameter, and Microphysics
1282 Flight-Level Data, Version 1.3 [Data set]. UCAR/NCAR - Earth Observing Laboratory.
1283 https://doi.org/10.5065/D6M32TM9
1284 UCAR/NCAR - Earth Observing Laboratory. (2020). UCAR/NCAR – Earth Observing
1285 Laboratory: VCSEL 1Hz Water Vapor Data Version 1.0 [Data set]. UCAR/NCAR -
1286 Earth Observing Laboratory. https://doi.org/10.26023/KFSD-Y8DQ-YC0D
1287 Ullrich, R., Hoose, C., Möhler, O., Niemand, M., Wagner, R., Höhler, K., et al. (2017). A New
1288 Ice Nucleation Active Site Parameterization for Desert Dust and Soot. *Journal of the*
1289 *Atmospheric Sciences*, *74*(3), 699–717. https://doi.org/10.1175/JAS-D-16-0074.1
1290 Vali, G. (1971). Quantitative Evaluation of Experimental Results on the Heterogeneous Freezing
1291 Nucleation of Supercooled Liquids. *Journal of the Atmospheric Sciences*, *28*(3), 402–409.
1292 https://doi.org/10.1175/1520-0469(1971)028<0402:QEOERA>2.0.CO;2
1293 Vergara-Temprado, J., Murray, B. J., Wilson, T. W., O'Sullivan, D., Browse, J., Pringle, K. J., et
1294 al. (2017). Contribution of feldspar and marine organic aerosols to global ice nucleating
1295 particle concentrations. *Atmospheric Chemistry and Physics*, *17*(5), 3637–3658.
1296 https://doi.org/10.5194/acp-17-3637-2017
1297 Vergara-Temprado, J., Miltenberger, A. K., Furtado, K., Grosvenor, D. P., Shipway, B. J., Hill,
1298 A. A., et al. (2018). Strong control of Southern Ocean cloud reflectivity by ice-nucleating
1299 particles. *Proceedings of the National Academy of Sciences*, *115*(11), 2687–2692.
1300 https://doi.org/10.1073/pnas.1721627115
1301 Wang, X., Deane, G. B., Moore, K. A., Ryder, O. S., Stokes, M. D., Beall, C. M., et al. (2017).
1302 The role of jet and film drops in controlling the mixing state of submicron sea spray

aerosol particles. *Proceedings of the National Academy of Sciences*, *114*(27), 6978–6983. https://doi.org/10.1073/pnas.1702420114

von der Weiden, S.-L., Drewnick, F., & Borrmann, S. (2009). Particle Loss Calculator – a new software tool for the assessment of the performance of aerosol inlet systems. *Atmospheric Measurement Techniques*, *2*(2), 479–494. https://doi.org/10.5194/amt-2-479-2009

Welti, A., Bigg, E. K., DeMott, P. J., Gong, X., Hartmann, M., Harvey, M., et al. (2020). Ship-based measurements of ice nuclei concentrations over the Arctic, Atlantic, Pacific and Southern oceans. *Atmospheric Chemistry and Physics*, *20*(23), 15191–15206. https://doi.org/10.5194/acp-20-15191-2020

Wilson, T. W., Ladino, L. A., Alpert, P. A., Breckels, M. N., Brooks, I. M., Browse, J., et al. (2015). A marine biogenic source of atmospheric ice-nucleating particles. *Nature*, *525*(7568), 234–238. https://doi.org/10.1038/nature14986

Zelinka, M. D., Myers, T. A., McCoy, D. T., Po-Chedley, S., Caldwell, P. M., Ceppi, P., et al. (2020). Causes of Higher Climate Sensitivity in CMIP6 Models. *Geophysical Research Letters*, *47*(1), e2019GL085782. https://doi.org/10.1029/2019GL085782

Zender, C. S., Bian, H., & Newman, D. (2003). Mineral Dust Entrainment and Deposition (DEAD) model: Description and 1990s dust climatology. *Journal of Geophysical Research: Atmospheres*, *108*(D14). https://doi.org/10.1029/2002JD002775

Zhao, X., Liu, X., Burrows, S., DeMott, P. J., Diao, M., McFarquhar, G. M., et al. (2023). Important Ice Processes Are Missed by the Community Earth System Model in Southern Ocean Mixed-Phase Clouds: Bridging SOCRATES Observations to Model Developments. *Journal of Geophysical Research: Atmospheres*, *128*(4), e2022JD037513. https://doi.org/10.1029/2022JD037513

1326